Light interaction with nano-materials

LUND
UNIVERSITY

Stylianos Tsopanidis

Supervisor: Prof. Hongqi Xu

Spring 2014

Contents

Abstract

"There is a crack in everything. That's how light gets in." With two simple sentences the famous poet Leonard Cohen describes his perception on how light interacts with matter. This thesis work will try to give a more precise and detailed description of the interaction between light and nano-materials that maybe is going to lose some of the magic that poetry has but this will be compensated by the magic of revealing how nature works through the physical phenomena.

The system that is studied in the current thesis consists of vertical periodic arrays of core-shell nanowires and the objective of the thesis is to simulate how the light interacts with this structure. The way to simulate the light propagation inside the system is to solve a set of differential equations, the well-known Maxwell equations. By solving these equations it becomes possible to calculate very important physical properties of the nano-structure that are connected to the efficiency of two main applications: the photovoltaic devices and photo-detectors. Moreover, different geometrical properties of the nano-structure (such as the shape of the nanowires, the diameter and the length of the nanowires, the periodicity of the arrays etc.) can be altered and the system can be studied for each different case. The results of the simulations can give useful information in order to find the structure that presents higher efficiency for the applications, but also to obtain a better understanding of the physical phenomena that are connected with light interaction with nano-materials.

It becomes obvious that simulations constitute a cost efficient method to investigate which structure has the potential to be used in a future application and to point the direction of a more extensive experimental research for these particular structures. In this way the experimental research becomes more effective and focused, with lower consumption of resources and time.

Chapter 1

Introduction

Optics and, more specifically, Photonics attract a considerable part of the scientific research, due to the numerous applications that these areas exhibit. Light interaction with all sort of materials, but mainly with nano-materials, is at the core of this research and by understanding the mechanism and the physical phenomena that govern this interaction scientists are in the position to create innovative efficient devices. Before getting into the applications, it is useful to start this introductory part with a short description of the process that is used to study the light interaction with nano-materials and argue about the advantages of the method.

Light is an electromagnetic wave; hence the study of the light propagation inside any medium should start by solving the set of Maxwell equations. Somewhere around 1861 James Clerk Maxwell published an early form of a set of four equations that became the most important formulae in the field of electromagnetism and electrodynamics. By solving these equations, for the boundary conditions of the system that is studied, one can obtain the values of the electric and the magnetic field in every position and it becomes possible to calculate very important properties of the system such as the absorptance, the transmittance, the reflectance etc.

The complexity of the system defines the level of difficulty of the problem. The system that is studied in this work consists of vertical periodic arrays of core-shell nanowires, where the light is incident normally on top of them and propagates until it reaches the SiO_2 substrate. The solutions of the Maxwell equations can only be obtained by employing numerical methods, using computer calculations. The detailed mathematical derivation of the method that is employed for the current thesis is presented in the theoretical overview

part of the thesis, using as a reference the scientific paper work of N.Anttu and H.Q.Xu, that was published on 2011 in the *Physical Review B* scientific magazine under the title *'Scattering matrix method for optical excitation of surface plasmons in metal films with periodic arrays of subwavelength holes'*.

A large amount of data should be handled in order to obtain the solutions of the set of Maxwell equations. Consequently, the numerical calculations can only be performed by a computer program. Therefore, a big part of this thesis work is to program an algorithm that manages the heavy calculations needed to be carried out to solve the set of equations for the particular system. Computer simulations have always been a very powerful tool for solving difficult equations and managing challenging theoretical calculations. The complexity of the system, that is of interest in this thesis, cannot allow us to solve the Maxwell equations with analytical methods and the numerical method, that is used instead can only be implemented with a computer program.

Similar work in simulations has already been done and published for structures of periodic vertical arrays of normal nanowires[2]. However, there is not enough information regarding the optical properties of the core-shell nanowires and this thesis will try to cover this gap. The published papers on normal nanowire array structures are used as a reference to compare the results of the core-shell nanowire system with. In addition, the previous papers are used to check the functionality of the algorithm created for the current work.

Finally, it is important to explain how this work can contribute to the improvement of devices such as photovoltaic and photo-detectors.

The main challenge of the scientific research devoted to photovoltaic devices has always been the increase of their efficiency and the goal is to reach the maximum efficiency with the smallest possible manufacturing cost. The material resources are finite and the reduction of the production cost is always a very demanding issue for the scientific research. This is one of the greatest advantages of the nano-structure that is of interest for this thesis. It is clear that a structure with periodic vertical arrays of nanowires needs less material than a thin film structure, that is currently used for the production of solar cells. Thus, it is important to know which geometry of the nano-structure yields high efficiency but also use as least as possible material resources. The diameter of the nanowires, the periodicity of the system and other geometrical properties are altered in order to find which structure presents higher absorptance with the minimum material usage. Moreover,

the core-shell nanowires exhibit additional advantages, due to their optical and electrical properties, and appear promising for these applications.

Furthermore, photo-detectors are sensors of light, with a big variety of different types and applications. Basically, the incoming light is absorbed by the detector and this results into a measurable photocurrent. The increase of the current is proportionally related to the absorption of light. Thus, the nano-structure of nanowire arrays, which exhibits a very high absorptance, makes possible to improve the performance of the photo-detectors. In addition, the system of the periodic nanowire arrays presents higher absorptance in certain frequencies of incoming light, due to the excitation of specific optical modes, and seems very promising for a chromo-detector, a sensor that identifies the wavelength or the frequency of the incoming light.

At last, this thesis is a theoretical work and the results of this work may give useful information for numerous applications and contribute to better understanding of the physics behind the light interaction with matter. It is very important, without any doubt, for the scientific research to be oriented towards to applicable areas, but it is also important to remember that physics is a science that mainly aims at giving a better understanding of the natural phenomena.

Chapter 2

Theory

The main objective of this thesis is to solve the set of Maxwell equations for a complex system constructed of vertical arrays of shell-core nanowires. By obtaining the solutions for the electric and the magnetic field, we are in a position to calculate properties of the system (such as the $Transmittance$, the $Reflectance$, the *Absorptance* e.t.c), that provide useful information for various applications of the system. The analytical solution of the equations is not an option when the system is as complex as the one that is of interest to the current work. Thus, the Maxwell equations should be solved by employing numerical computation methods. The most important methods that usually are used for solving the equations are[6]:

- The Finite Element Method (FEM) and the Finite Difference Time Domain method (FDTD) are the most important space domain methods. The Maxwell equations are represented as partial differential equations in a space domain and the values of the electromagnetic fields at discrete spatial points are calculated.
- Fourier Modal Method (FMM), which is a spatial frequency domain method.

The method that is used for this thesis is the Fourier modal method[7],[10],[12]. The Maxwell equations are re-formulated into an eigenvalue matrix equation and the electric and magnetic fields are expanded onto an orthonormal Bloch basis. The symmetry of the periodic system allows to represent the electric and the magnetic field in Bloch eigenmodes, where each eigenmode is an expansion in pseudo-Fourier series[6]. By using this method it becomes possible

to obtain the general solutions of the Maxwell equations for the different areas of the system.

In addition, the transfer matrix method and the scattering matrix method provide the mathematical formalism that interconnects the solutions from each individual area in order to calculate the electric and the magnetic field in every position of the whole system.

In most of the publications, in scientific magazines and journals, the intermediate steps of these methods are not presented rigorously due to the limited space of a scientific paper or the fact that the author is usually more interested in presenting the results rather than providing a detailed mathematical derivation. Therefore, in this chapter the entire mathematical process of the implementation of these methods for solving the Maxwell equations for this particular system will be carried out.

Initially, the mathematical formalism for a general arbitrary system is presented and then the method is implemented on the particular system of the nano-structure that is of interest for this thesis.

2.1 Fourier Modal Method

First of all, the system is divided into different areas along the propagation of light. The light is assumed to be a plane wave that propagates along the z direction and impinges on the left or the right side of the system. In every slice of the system we consider that the permittivity $\tilde{\epsilon}$ is constant along the z direction. Since the permittivity is dependent on the material, it is easy to conclude that the division of the system is done in a way that every slice consists of the same material along the z direction, even though it may have different material structure along x or y direction. A schematic of this arbitrary system can be seen in Fig. 2.1

The Maxwell equations have the following form:

$$\nabla \times \mathbf{E}(\mathbf{r}, \omega) = -\frac{\partial \mathbf{B}(\mathbf{r}, \omega)}{\partial t}$$

$$\nabla \times \mathbf{H}(\mathbf{r}, \omega) = \frac{\partial \mathbf{D}(\mathbf{r}, \omega)}{\partial t}$$

$$\nabla \cdot \mathbf{B}(\mathbf{r}, \omega) = 0$$

$$\nabla \cdot \mathbf{D}(\mathbf{r}, \omega) = 0$$

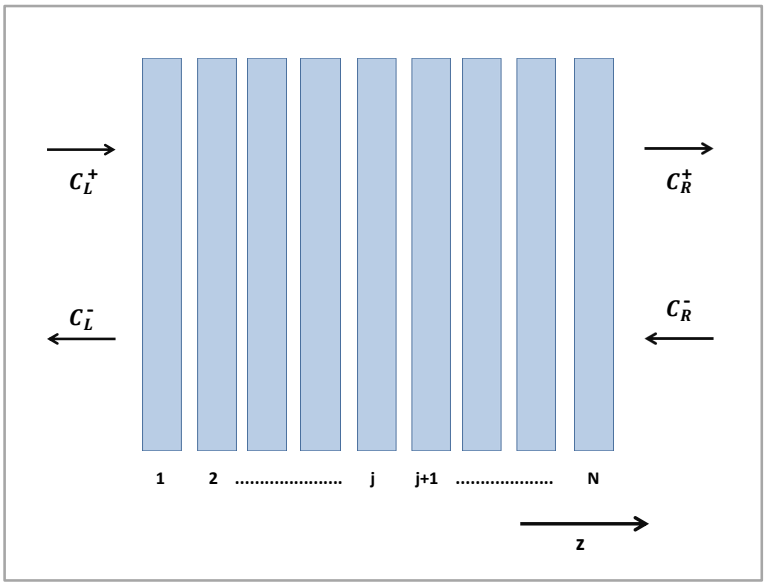

Figure 2.1: The system is divided into N different slices. In every slice the permittivity remains constant along the z direction, but it could change along the xy-plane. Light is incident on the left or the right side of the structure.

where ω is the frequency of the light and $\mathbf{E}$, $\mathbf{D}$, $\mathbf{B}$ and $\mathbf{H}$ represent the electric field, the electric displacement, the magnetic induction and the magnetic field, respectively. If we substitute the electric displacement and the magnetic induction according to the following:

$$\mathbf{D}(\mathbf{r},\omega) = \tilde{\epsilon}(\mathbf{r},\omega)\mathbf{E}(\mathbf{r},\omega)$$
$$\mathbf{B}(\mathbf{r},\omega) = \tilde{\mu}(\mathbf{r},\omega)\mathbf{H}(\mathbf{r},\omega)$$

we end up with:

$$\nabla \times \mathbf{E}(\mathbf{r},\omega) = -\frac{\partial(\tilde{\mu}(\mathbf{r},\omega)\mathbf{H}(\mathbf{r},\omega))}{\partial t}$$
$$\nabla \times \mathbf{H}(\mathbf{r},\omega) = \frac{\partial(\tilde{\epsilon}(\mathbf{r},\omega)\mathbf{E}(\mathbf{r},\omega))}{\partial t}$$
$$\nabla \cdot (\tilde{\mu}(\mathbf{r},\omega)\mathbf{H}(\mathbf{r},\omega)) = 0$$
$$\nabla \cdot (\tilde{\epsilon}(\mathbf{r},\omega)\mathbf{E}(\mathbf{r},\omega)) = 0$$

Finally, if we consider time harmonic electromagnetic fields, the Maxwell equations become:

$$\nabla \times \mathbf{E}(\mathbf{r},\omega) = i\omega\tilde{\mu}(\mathbf{r},\omega)\mathbf{H}(\mathbf{r},\omega) \tag{2.2a}$$
$$\nabla \times \mathbf{H}(\mathbf{r},\omega) = -i\omega\tilde{\epsilon}(\mathbf{r},\omega)\mathbf{E}(\mathbf{r},\omega) \tag{2.2b}$$
$$\nabla \cdot (\tilde{\mu}(\mathbf{r},\omega)\mathbf{H}(\mathbf{r},\omega)) = 0 \tag{2.2c}$$
$$\nabla \cdot (\tilde{\epsilon}(\mathbf{r},\omega)\mathbf{E}(\mathbf{r},\omega)) = 0 \tag{2.2d}$$

The calculations will be carried out for a certain frequency ω of the incoming light each time, hence, we are allowed to skip ω from the notation. The permittivity $\tilde{\epsilon}$ can be calculated from the complex index of refraction ($\tilde{n} = n + ik$) of the material according to the following formula:

$$\tilde{\epsilon} = \epsilon_0\tilde{\epsilon_r} = \epsilon_0\tilde{n}^2$$

where ϵ_0 is the permittivity of the vacuum. Thus, the relative permittivity $\tilde{\epsilon_r}$ is a complex number ($\tilde{\epsilon_r} = \epsilon_1 + i\epsilon_2$) with real part: $\epsilon_1 = n^2 - k^2$ and imaginary part: $\epsilon_2 = 2nk$.

Given that the permittivity is z-independent, the notation that is used is $\tilde{\epsilon}(x, y)$ and it is clear that the permittivity changes only on the x and y direction inside each slice.

Moreover, the permeability that appears in Maxwell equations is considered to be equal to the permeability of the free space $\tilde{\mu}(r,\omega) = \tilde{\mu} = \mu_0$ because the materials that are of interest for this thesis are non-magnetic materials.

Since the system is divided into different areas, the electric field in the jth area is denoted as $\mathbf{E}^j$ and the magnetic field as $\mathbf{H}^j$. Starting with the eq. 2.2a it is easy to obtain the following set of equations:

$$\frac{\partial}{\partial z}E_y^j(\mathbf{r}) = -i\omega\tilde{\mu}_j H_x^j(\mathbf{r}) + \frac{\partial}{\partial y}E_z^j(\mathbf{r}) \tag{2.3a}$$
$$\frac{\partial}{\partial z}E_x^j(\mathbf{r}) = i\omega\tilde{\mu}_j H_y^j(\mathbf{r}) + \frac{\partial}{\partial x}E_z^j(\mathbf{r}) \tag{2.3b}$$
$$H_z^j(\mathbf{r}) = \frac{1}{i\omega\tilde{\mu}_j}\left(\frac{\partial}{\partial x}E_y^j(\mathbf{r}) - \frac{\partial}{\partial y}E_x^j(\mathbf{r})\right) \tag{2.3c}$$

Similarly, from the eq. 2.2b:

$$\frac{\partial}{\partial z}H_y^j(\mathbf{r}) = i\omega\tilde{\epsilon}_j(x,y)E_x^j(\mathbf{r}) + \frac{\partial}{\partial y}H_z^j(\mathbf{r}) \tag{2.4a}$$

$$\frac{\partial}{\partial z}H_x^j(\mathbf{r}) = -i\omega\tilde{\epsilon}_j(x,y)E_y^j(\mathbf{r}) + \frac{\partial}{\partial x}H_z^j(\mathbf{r}) \tag{2.4b}$$

$$E_z^j(\mathbf{r}) = -\frac{1}{i\omega\tilde{\epsilon}_j(x,y)}\left(\frac{\partial}{\partial x}H_y^j(\mathbf{r}) - \frac{\partial}{\partial y}H_x^j(\mathbf{r})\right) \tag{2.4c}$$

If we substitute eq. 2.4c to the equations 2.3a and 2.3b, we get:

$$\frac{\partial}{\partial z}E_y^j(\mathbf{r}) = \left(\frac{1}{i\omega}\frac{\partial}{\partial y}\frac{1}{\tilde{\epsilon}_j(x,y)}\frac{\partial}{\partial y} - i\omega\tilde{\mu}_j\right)H_x^j(\mathbf{r}) - \frac{1}{i\omega}\frac{\partial}{\partial y}\frac{1}{\tilde{\epsilon}_j(x,y)}\frac{\partial}{\partial x}H_y^j(\mathbf{r}) \tag{2.5a}$$

$$\frac{\partial}{\partial z}E_x^j(\mathbf{r}) = \frac{1}{i\omega}\frac{\partial}{\partial x}\frac{1}{\tilde{\epsilon}_j(x,y)}\frac{\partial}{\partial y}H_x^j(\mathbf{r}) + \left(i\omega\tilde{\mu}_j - \frac{1}{i\omega}\frac{\partial}{\partial x}\frac{1}{\tilde{\epsilon}_j(x,y)}\frac{\partial}{\partial x}\right)H_y^j(\mathbf{r}) \tag{2.5b}$$

By substituting eq. 2.3c to the equations 2.4a and 2.4b, we end up with :

$$\frac{\partial}{\partial z}H_y^j(\mathbf{r}) = \left(i\omega\tilde{\epsilon}_j(x,y) - \frac{1}{i\omega}\frac{\partial}{\partial y}\frac{1}{\tilde{\mu}}\frac{\partial}{\partial y}\right)E_x^j(\mathbf{r}) + \frac{1}{i\omega}\frac{\partial}{\partial y}\frac{1}{\tilde{\mu}}\frac{\partial}{\partial x}E_y^j(\mathbf{r}) \tag{2.6a}$$

$$\frac{\partial}{\partial z}H_x^j(\mathbf{r}) = -\frac{1}{i\omega}\frac{\partial}{\partial x}\frac{1}{\tilde{\mu}}\frac{\partial}{\partial y}E_x^j(\mathbf{r}) + \left(-i\omega\tilde{\epsilon}_j(x,y) + \frac{1}{i\omega}\frac{\partial}{\partial x}\frac{1}{\tilde{\mu}}\frac{\partial}{\partial x}\right)E_y^j(\mathbf{r}) \tag{2.6b}$$

Finally, these four equations (eq. 2.5a, eq. 2.5b,eq. 2.6a and eq. 2.6b) can be written in matrix form as follows [1],[11]:

$$\frac{\partial}{\partial z}\begin{bmatrix}E_x^j(\mathbf{r})\\E_y^j(\mathbf{r})\end{bmatrix} = \hat{\mathbf{T}}_1^j\begin{bmatrix}H_x^j(\mathbf{r})\\H_y^j(\mathbf{r})\end{bmatrix} \tag{2.7}$$

$$\frac{\partial}{\partial z}\begin{bmatrix}H_x^j(\mathbf{r})\\H_y^j(\mathbf{r})\end{bmatrix} = \hat{\mathbf{T}}_2^j\begin{bmatrix}E_x^j(\mathbf{r})\\E_y^j(\mathbf{r})\end{bmatrix} \tag{2.8}$$

Where the operators $\hat{\mathbf{T}}_1^j$ and $\hat{\mathbf{T}}_2^j$ are :

$$\hat{\mathbf{T}}_1^j = \begin{bmatrix} \hat{\mathbf{T}}_{1,xx}^j & \hat{\mathbf{T}}_{1,xy}^j \\ \hat{\mathbf{T}}_{1,yx}^j & \hat{\mathbf{T}}_{1,yy}^j \end{bmatrix} \tag{2.9a}$$

$$\hat{\mathbf{T}}_2^j = \begin{bmatrix} \hat{\mathbf{T}}_{2,xx}^j & \hat{\mathbf{T}}_{2,xy}^j \\ \hat{\mathbf{T}}_{2,yx}^j & \hat{\mathbf{T}}_{2,yy}^j \end{bmatrix} \tag{2.9b}$$

The matrix elements of the operator $\hat{\mathbf{T}}_1^j$ are :

$$\hat{\mathbf{T}}_{1,xx}^j = \frac{1}{i\omega}\frac{\partial}{\partial x}\frac{1}{\tilde{\epsilon}_j(x,y)}\frac{\partial}{\partial y} \tag{2.10}$$

$$\hat{\mathbf{T}}_{1,xy}^j = i\omega\tilde{\mu}_j(x,y) - \frac{1}{i\omega}\frac{\partial}{\partial x}\frac{1}{\tilde{\epsilon}_j(x,y)}\frac{\partial}{\partial x} \tag{2.11}$$

$$\hat{\mathbf{T}}_{1,yx}^j = -i\omega\tilde{\mu}_j(x,y) + \frac{1}{i\omega}\frac{\partial}{\partial y}\frac{1}{\tilde{\epsilon}_j(x,y)}\frac{\partial}{\partial y} \tag{2.12}$$

$$\hat{\mathbf{T}}_{1,yy}^j = -\frac{1}{i\omega}\frac{\partial}{\partial y}\frac{1}{\tilde{\epsilon}_j(x,y)}\frac{\partial}{\partial x} \tag{2.13}$$

Similarly, for the operator $\hat{\mathbf{T}}_2^j$:

$$\hat{\mathbf{T}}_{2,xx}^j = -\frac{1}{i\omega}\frac{\partial}{\partial x}\frac{1}{\tilde{\mu}_j(x,y)}\frac{\partial}{\partial y} \tag{2.14}$$

$$\hat{\mathbf{T}}_{2,xy}^j = -i\omega\tilde{\epsilon}_j(x,y) + \frac{1}{i\omega}\frac{\partial}{\partial x}\frac{1}{\tilde{\mu}_j(x,y)}\frac{\partial}{\partial x} \tag{2.15}$$

$$\hat{\mathbf{T}}_{2,yx}^j = i\omega\tilde{\epsilon}_j(x,y) - \frac{1}{i\omega}\frac{\partial}{\partial y}\frac{1}{\tilde{\mu}_j(x,y)}\frac{\partial}{\partial y} \tag{2.16}$$

$$\hat{\mathbf{T}}_{2,yy}^j = \frac{1}{i\omega}\frac{\partial}{\partial y}\frac{1}{\tilde{\mu}_j(x,y)}\frac{\partial}{\partial x} \tag{2.17}$$

By combining the equations 2.7 and 2.8:

$$\frac{\partial^2}{\partial z^2}\begin{bmatrix} E_x^j(\mathbf{r}) \\ E_y^j(\mathbf{r}) \end{bmatrix} = \hat{\mathbf{T}}_1^j\hat{\mathbf{T}}_2^j\begin{bmatrix} E_x^j(\mathbf{r}) \\ E_y^j(\mathbf{r}) \end{bmatrix} \tag{2.18}$$

The possible solutions of this equation are eigenmodes of the form[1]:

$$\tilde{\mathbf{E}}_j^{\alpha}(\mathbf{r}) = \tilde{\mathbf{E}}_j^{\alpha}(x,y)e^{\pm k_j^{\alpha}(z-z_j)} = \begin{bmatrix} \tilde{E}_{j,x}^{\alpha}(x,y) \\ \tilde{E}_{j,y}^{\alpha}(x,y) \end{bmatrix} e^{\pm k_j^{\alpha}(z-z_j)}$$

Substituting that into the eq.2.18, gives:

$$-(k_j^{\alpha})^2 \begin{bmatrix} \tilde{E}_{j,x}^{\alpha}(x,y) \\ \tilde{E}_{j,y}^{\alpha}(x,y) \end{bmatrix} = \hat{\mathbf{T}}_1^j \hat{\mathbf{T}}_2^j \begin{bmatrix} \tilde{E}_{j,x}^{\alpha}(x,y) \\ \tilde{E}_{j,y}^{\alpha}(x,y) \end{bmatrix}$$

Now, we can expand $\tilde{\mathbf{E}}_j^{\alpha}(x,y)$ in a complete, orthonormal basis, $\{\phi_n(x,y)\}$ and write the components as :

$$\tilde{E}_{j,x(y)}^{\alpha}(x,y) = \sum_m d_{j,x(y),m}^{\alpha} \phi_m(x,y)$$

Using this, results in the following matrix eigenvalue equation:

$$\beta_j^{\alpha} \mathbf{d}_j^{\alpha} = -\mathbf{T}_1^j \mathbf{T}_2^j \mathbf{d}_j^{\alpha} \tag{2.19}$$

Where $\beta_j^{\alpha} = (k_j^{\alpha})^2$. The $\mathbf{T}_1^j$ and $\mathbf{T}_2^j$ are operators of a matrix form. These operator matrices are the result of the projection of the operators $\hat{\mathbf{T}}_1^j$ and $\hat{\mathbf{T}}_2^j$ onto the orthonormal basis $\{\phi_n(x,y)\}$. Thus, the matrix elements of the submatrices that the operator matrix $\mathbf{T}_{1(2)}^j$ is constructed of, can be obtained from: $[\mathbf{T}_{1(2),ll'}^j]_{m,n} = < \phi_m | \hat{\mathbf{T}}_{1(2),ll'}^j | \phi_n >$.

The electric field expansion coefficients that appear in eq. 2.19 are written in the following vector form:

$$\mathbf{d}_j^{\alpha} = \begin{bmatrix} \mathbf{d}_{j,x}^{\alpha} \\ \mathbf{d}_{j,y}^{\alpha} \end{bmatrix}$$

By solving the eigenvalue equation, it is possible to calculate the eigenvalues and eigenvectors for each area of the system.

The general solution for the electric field $\mathbf{E}^j(\mathbf{r})$ of the jth slice is the superposition of the solutions of all eigenmodes and its components can be expressed as [9]:

$$E_x^j(\mathbf{r}) = \sum_\alpha \tilde{E}_{j,x}^\alpha(x,y)[C_j^{+,\alpha} e^{ik_j^\alpha(z-z_j)} + C_j^{-,\alpha} e^{-ik_j^\alpha(z-z_j)}] = \\ = \sum_\alpha \sum_m d_{j,x,m}^\alpha \phi_m(x,y)[C_j^{+,\alpha} e^{ik_j^\alpha(z-z_j)} + C_j^{-,\alpha} e^{-ik_j^\alpha(z-z_j)}] \tag{2.20}$$

$$E_y^j(\mathbf{r}) = \sum_\alpha \tilde{E}_{j,y}^\alpha(x,y)[C_j^{+,\alpha} e^{ik_j^\alpha(z-z_j)} + C_j^{-,\alpha} e^{-ik_j^\alpha(z-z_j)}] = \\ = \sum_\alpha \sum_m d_{j,y,m}^\alpha \phi_m(x,y)[C_j^{+,\alpha} e^{ik_j^\alpha(z-z_j)} + C_j^{-,\alpha} e^{-ik_j^\alpha(z-z_j)}] \tag{2.21}$$

The wave vectors k_j^α are complex numbers and they can be calculated from the eigenvalues ($k_j^\alpha = \sqrt{\beta_j^\alpha}$) of the eigenvalue equation (eq. 2.19). These values of the wave vectors should have positive real part, if the imaginary part is zero, and positive imaginary part, if the imaginary part is non-zero[1]. By applying these conditions, the expansion coefficients $\{C_j^{+,\alpha}\}$ represent two types of modes: the modes that are propagating forward or the modes that are exponentially decaying along the z direction. Similarly, the expansion coefficients $\{C_j^{-,\alpha}\}$ represent modes that are either propagating backwards or exponentially growing along the z direction.

Additionally, the general solution for the magnetic field $\mathbf{H}^j(\mathbf{r})$ for the jth slice has components:

$$H_x^j(\mathbf{r}) = \sum_\alpha \sum_m h_{j,x,m}^\alpha \phi_m(x,y)[C_j^{+,\alpha} e^{ik_j^\alpha(z-z_j)} - C_j^{-,\alpha} e^{-ik_j^\alpha(z-z_j)}] \tag{2.22}$$

$$H_y^j(\mathbf{r}) = \sum_\alpha \sum_m h_{j,y,m}^\alpha \phi_m(x,y)[C_j^{+,\alpha} e^{ik_j^\alpha(z-z_j)} - C_j^{-,\alpha} e^{-ik_j^\alpha(z-z_j)}] \tag{2.23}$$

The magnetic field expansion coefficients are:

$$\mathbf{h}_j^\alpha = \begin{bmatrix} \mathbf{h}_{j,x}^\alpha \\ \mathbf{h}_{j,y}^\alpha \end{bmatrix} = ik_j^\alpha \left(\mathbf{T}_1^j\right)^{-1} \mathbf{d}_j^\alpha \tag{2.24}$$

In conclusion, by using the Fourier Modal Method it becomes possible to solve the Maxwell equations and derive an equation for the general solutions for the electric and the magnetic field inside each slice of the system. For these solutions, only the expansion coefficients $\{C_j^{+,\alpha}\}$ and $\{C_j^{-,\alpha}\}$ remain unknown. By using the Transfer Matrix Method and the Scattering Matrix Method it becomes possible to calculate these expansion coefficients and obtain the solutions for the electric and the magnetic field.

2.2 Transfer and Scattering Matrix Method

The expansion coefficients $\{C_j^{+,\alpha}\}$ and $\{C_j^{-,\alpha}\}$, that appear in the general solutions of the electric and the magnetic field, are known for the incoming light. In order to calculate the expansion coefficients for the rest of the areas of the system, it is necessary to find a way to connect the expansion coefficients of each area with the expansion coefficients of the adjacent area. Consequently, the next step of the calculations is to connect the expansion coefficients of the slice j ($\{C_j^{+,\alpha}\}$ and $\{C_j^{-,\alpha}\}$) to the expansion coefficients of the next slice ($\{C_{j+1}^{+,\alpha}\}$ and $\{C_{j+1}^{-,\alpha}\}$).

From Maxwell equations, considering the time harmonic dependence of the electromagnetic fields, one has that the transverse components of the electric and magnetic field are continuous at the interface between two adjacent slices:

$$\begin{bmatrix} \mathbf{E}_x^{j+1}(\mathbf{r}) \\ \mathbf{E}_y^{j+1}(\mathbf{r}) \end{bmatrix} = \begin{bmatrix} \mathbf{E}_x^{j}(\mathbf{r}) \\ \mathbf{E}_y^{j}(\mathbf{r}) \end{bmatrix}$$

and

$$\begin{bmatrix} \mathbf{H}_x^{j+1}(\mathbf{r}) \\ \mathbf{H}_y^{j+1}(\mathbf{r}) \end{bmatrix} = \begin{bmatrix} \mathbf{H}_x^{j}(\mathbf{r}) \\ \mathbf{H}_y^{j}(\mathbf{r}) \end{bmatrix}$$

It is possible to write the above equations in a matrix form, using the expansion coefficients, as follows:

$$\begin{bmatrix} \mathbf{P}_{j+1} & \mathbf{P}_{j+1} \\ \mathbf{Q}_{j+1} & -\mathbf{Q}_{j+1} \end{bmatrix} \begin{bmatrix} \mathbf{C}_{j+1}^{+} \\ \mathbf{C}_{j+1}^{-} \end{bmatrix} = \begin{bmatrix} \mathbf{P}_{j} & \mathbf{P}_{j} \\ \mathbf{Q}_{j} & -\mathbf{Q}_{j} \end{bmatrix} \begin{bmatrix} \boldsymbol{\gamma}_j & \mathbf{0} \\ \mathbf{0} & \boldsymbol{\gamma}_j^{-1} \end{bmatrix} \begin{bmatrix} \mathbf{C}_{j}^{+} \\ \mathbf{C}_{j}^{-} \end{bmatrix} \tag{2.25}$$

where

$$(\mathbf{P}_j)_{n\alpha} = (\mathbf{d}_j^{\alpha})_n \tag{2.26}$$

$$(\mathbf{Q}_j)_{n\alpha} = (\mathbf{h}_j^{\alpha})_n \tag{2.27}$$

$$(\boldsymbol{\gamma}_j)_{m\alpha} = \delta_{m,\alpha} e^{ik_j^{\alpha}(z_{j+1}-z_j)} \tag{2.28}$$

By multiplying with the inverse matrices, the previous equation for the coefficients in the jth slice yields:

$$\begin{bmatrix} \mathbf{C}_j^+ \\ \mathbf{C}_j^- \end{bmatrix} = \begin{bmatrix} \boldsymbol{\gamma}_j & \mathbf{0} \\ \mathbf{0} & \boldsymbol{\gamma}_j^{-1} \end{bmatrix}^{-1} \begin{bmatrix} \mathbf{P}_j & \mathbf{P}_j \\ \mathbf{Q}_j & -\mathbf{Q}_j \end{bmatrix}^{-1} \begin{bmatrix} \mathbf{P}_{j+1} & \mathbf{P}_{j+1} \\ \mathbf{Q}_{j+1} & -\mathbf{Q}_{j+1} \end{bmatrix} \begin{bmatrix} \mathbf{C}_{j+1}^+ \\ \mathbf{C}_{j+1}^- \end{bmatrix} \tag{2.29}$$

And we end up with:

$$\begin{bmatrix} \mathbf{C}_j^+ \\ \mathbf{C}_j^- \end{bmatrix} = \begin{bmatrix} \mathbf{M}_{11}(j, j+1) & \mathbf{M}_{12}(j, j+1) \\ \mathbf{M}_{21}(j, j+1) & \mathbf{M}_{22}(j, j+1) \end{bmatrix} \begin{bmatrix} \mathbf{C}_{j+1}^+ \\ \mathbf{C}_{j+1}^- \end{bmatrix} \tag{2.30}$$

where $\mathbf{M}(j, j+1)$ is the transfer matrix, with elements the following submatrices:

$$\mathbf{M}_{11}(j, j+1) = \boldsymbol{\gamma^{-1}}_j \mathbf{T}_{11}(j, j+1) \tag{2.31a}$$
$$\mathbf{M}_{12}(j, j+1) = \boldsymbol{\gamma^{-1}}_j \mathbf{T}_{12}(j, j+1) \tag{2.31b}$$
$$\mathbf{M}_{21}(j, j+1) = \boldsymbol{\gamma}_j \mathbf{T}_{12}(j, j+1) \tag{2.31c}$$
$$\mathbf{M}_{11}(j, j+1) = \boldsymbol{\gamma}_j \mathbf{T}_{11}(j, j+1) \tag{2.31d}$$

with

$$\mathbf{T}_{11}(j, j+1) = \frac{1}{2}(\mathbf{P}_j^{-1}\mathbf{P}_{j+1} + \mathbf{Q}_j^{-1}\mathbf{Q}_{j+1}) \tag{2.32a}$$
$$\mathbf{T}_{11}(j, j+1) = \frac{1}{2}(\mathbf{P}_j^{-1}\mathbf{P}_{j+1} - \mathbf{Q}_j^{-1}\mathbf{Q}_{j+1}) \tag{2.32b}$$

Furthermore, by following the same process it is possible to calculate the expansion coefficients of the j-1 slice or the j+2 slice and in the end we can

calculate the total transfer matrix, that is the product of transfer matrices for all the interfaces between the adjacent slices. We assume that on the left and the right side of the structure there are two semi-infinite, homogeneous areas. By denoting as $\{C_L^{+,\alpha}\}$ and $\{C_L^{-,\alpha}\}$ the expansion coefficients of the incoming and outgoing light waves of the left side of the system and as $\{C_R^{+,\alpha}\}$ and $\{C_R^{-,\alpha}\}$ the expansion coefficients of the incoming and outgoing light waves of the right side of the system, it is possible to write a matrix equation for the entire system.

$$\begin{bmatrix} \mathbf{C}_L^+ \\ \mathbf{C}_L^- \end{bmatrix} = \mathbf{M}(L,R) \begin{bmatrix} \mathbf{C}_R^+ \\ \mathbf{C}_R^- \end{bmatrix}$$

where in this case $\mathbf{M}(L,R)$ is the total transfer matrix that couples the expansion coefficients of the left side with the expansion coefficients of the right side.

However, the exponential factors inside the $\boldsymbol{\gamma}_j$ and $\boldsymbol{\gamma}_j^{-1}$ can possibly cause numerical instability in the computer calculations. To overcome this one should approach the calculations using the scattering matrix method, instead of the transfer matrix method.[15],[16],[18],[17] The difference in the scattering matrix method is that the coupling is between the incoming light waves $\{C_R^{+,\alpha}\}$ and $\{C_L^{-,\alpha}\}$ with the outgoing waves $\{C_L^{+,\alpha}\}$ and $\{C_R^{-,\alpha}\}$:

$$\begin{bmatrix} \mathbf{C}_R^+ \\ \mathbf{C}_L^- \end{bmatrix} = \mathbf{S}(L,R) \begin{bmatrix} \mathbf{C}_L^+ \\ \mathbf{C}_R^- \end{bmatrix} = \begin{bmatrix} \mathbf{S}_{11}(L,R) & \mathbf{S}_{12}(L,R) \\ \mathbf{S}_{21}(L,R) & \mathbf{S}_{22}(L,R) \end{bmatrix} \begin{bmatrix} \mathbf{C}_L^+ \\ \mathbf{C}_R^- \end{bmatrix} \tag{2.33}$$

the $\mathbf{S}(L,R)$ is called the total scattering matrix of the system. This matrix can be obtained from the transfer matrices, by applying an iteration process similar to the one that we followed in order to get the total transfer matrix.

Firstly, we assume the subsystem that begins from the left homogeneous area and finishes to the arbitrary jth slice. The following equation describes this subsystem :

$$\begin{bmatrix} \mathbf{C}_j^+ \\ \mathbf{C}_L^- \end{bmatrix} = \mathbf{S}(L,j) \begin{bmatrix} \mathbf{C}_L^+ \\ \mathbf{C}_j^- \end{bmatrix} = \begin{bmatrix} \mathbf{S}_{11}(L,j) & \mathbf{S}_{12}(L,j) \\ \mathbf{S}_{21}(L,j) & \mathbf{S}_{22}(L,j) \end{bmatrix} \begin{bmatrix} \mathbf{C}_L^+ \\ \mathbf{C}_j^- \end{bmatrix} \tag{2.34}$$

the $\mathbf{S}(L,j)$ is the transfer matrix of the subsystem.

The sub-matrices of the scattering matrix can be derived from the transfer matrices by combining this equation (eq.2.34) with the equation 2.30. Thus,

the sub-matrices take the form [15]:

$$\begin{aligned}
\mathbf{S}_{11}(L,j+1) &= [\mathbf{I}-\mathbf{M}_{11}^{-1}(j,j+1)\mathbf{S}_{12}(L,j)\mathbf{M}_{21}(j,j+1)]^{-1}\mathbf{M}_{11}^{-1}(j,j+1)\mathbf{S}_{11}(L,j)\\
\mathbf{S}_{12}(L,j+1) &= [\mathbf{I}-\mathbf{M}_{11}^{-1}(j,j+1)\mathbf{S}_{12}(L,j)\mathbf{M}_{21}(j,j+1)]^{-1}\\
&\quad\times[\mathbf{M}_{11}^{-1}(j,j+1)\mathbf{S}_{12}(L,j)\mathbf{M}_{22}(j,j+1)-\mathbf{M}_{11}^{-1}(j,j+1)\mathbf{M}_{12}(j,j+1)]\\
\mathbf{S}_{21}(L,j+1) &= \mathbf{S}_{22}(L,j)\mathbf{M}_{21}(j,j+1)\mathbf{S}_{11}(L,j+1)+\mathbf{S}_{21}(L,j)\\
\mathbf{S}_{22}(L,j+1) &= \mathbf{S}_{22}(L,j)\mathbf{M}_{21}(j,j+1)\mathbf{S}_{12}(L,j+1)+\mathbf{S}_{22}(L,j)\mathbf{M}_{22}(j,j+1)
\end{aligned}$$

Substituting the matrix elements of the transfer matrix according the equations 2.31 and 2.32 gives:

$$\mathbf{S}_{11}(L,j{+}1) = \Big[\mathbf{I}-\left(\boldsymbol{\gamma}_j^{-1}\mathbf{T}_{11}(j,j+1)\right)^{-1}\mathbf{S}_{12}(L,j)\left(\boldsymbol{\gamma}_j\mathbf{T}_{12}(j,j+1)\right)\Big]^{-1}\left(\boldsymbol{\gamma}_j^{-1}\mathbf{T}_{11}(j,j+1)\right)^{-1}\mathbf{S}_{11}(L,j)$$

$$\begin{aligned}
\mathbf{S}_{12}(L,j+1) &= \Big[\mathbf{I}-\left(\boldsymbol{\gamma}_j^{-1}\mathbf{T}_{11}(j,j+1)\right)^{-1}\mathbf{S}_{12}(L,j)\left(\boldsymbol{\gamma}_j\mathbf{T}_{12}(j,j+1)\right)\Big]^{-1}\\
&\quad\times\Big[\left(\boldsymbol{\gamma}_j^{-1}\mathbf{T}_{11}(j,j+1)\right)^{-1}\mathbf{S}_{12}(L,j)\left(\boldsymbol{\gamma}_j\mathbf{T}_{11}(j,j+1)\right)-\left(\boldsymbol{\gamma}_j^{-1}\mathbf{T}_{11}(j,j+1)\right)^{-1}\left(\boldsymbol{\gamma}_j^{-1}\mathbf{T}_{12}(j,j+1)\right)\Big]
\end{aligned}$$

$$\mathbf{S}_{21}(L,j+1) = \mathbf{S}_{22}(L,j)\left(\boldsymbol{\gamma}_j\mathbf{T}_{12}(j,j+1)\right)\mathbf{S}_{11}(L,j+1)+\mathbf{S}_{21}(L,j)$$

$$\mathbf{S}_{22}(L,j+1) = \mathbf{S}_{22}(L,j)\left(\boldsymbol{\gamma}_j\mathbf{T}_{12}(j,j+1)\right)\mathbf{S}_{12}(L,j+1)+\mathbf{S}_{22}(L,j)\left(\boldsymbol{\gamma}_j\mathbf{T}_{11}(j,j+1)\right)$$

By using the mathematical properties of inverse matrices :

$$[\mathbf{AB}]^{-1} = \mathbf{B}^{-1}\mathbf{A}^{-1}$$

and

$$\boldsymbol{\gamma}_j\boldsymbol{\gamma}_j^{-1} = \mathbf{1}$$

we derive:

$$\mathbf{S}_{11}(L,j+1) = \left[\mathbf{I} - \mathbf{T}_{11}^{-1}(j,j+1)\boldsymbol{\gamma}_j\mathbf{S}_{12}(L,j)\boldsymbol{\gamma}_j\mathbf{T}_{12}(j,j+1)\right]^{-1}\mathbf{T}_{11}^{-1}(j,j+1)\boldsymbol{\gamma}_j\mathbf{S}_{11}(L,j) \tag{2.36a}$$

$$\begin{aligned}\mathbf{S}_{12}(L,j+1) = &\left[\mathbf{I} - \mathbf{T}_{11}^{-1}(j,j+1)\boldsymbol{\gamma}_j\mathbf{S}_{12}(L,j)\boldsymbol{\gamma}_j\mathbf{T}_{12}(j,j+1)\right]^{-1} \\ &\times\left[\mathbf{T}_{11}^{-1}(j,j+1)\boldsymbol{\gamma}_j\mathbf{S}_{12}(L,j)\boldsymbol{\gamma}_j\mathbf{T}_{11}(j,j+1) - \mathbf{T}_{11}^{-1}(j,j+1)\mathbf{T}_{12}(j,j+1)\right]\end{aligned} \tag{2.36b}$$

$$\mathbf{S}_{21}(L,j+1) = \mathbf{S}_{22}(L,j)\boldsymbol{\gamma}_j\mathbf{T}_{12}(j,j+1)\mathbf{S}_{11}(L,j+1) + \mathbf{S}_{21}(L,j) \tag{2.36c}$$

$$\mathbf{S}_{22}(L,j+1) = \mathbf{S}_{22}(L,j)\boldsymbol{\gamma}_j\mathbf{T}_{12}(j,j+1)\mathbf{S}_{12}(L,j+1) + \mathbf{S}_{22}(L,j)\boldsymbol{\gamma}_j\mathbf{T}_{11}(j,j+1) \tag{2.36d}$$

Hence, it becomes clear that using the scattering matrix method we accomplish to do the calculations without the need of calculating the $\boldsymbol{\gamma}_j^{-1}$ matrix which contains the exponentially growing factors that are the source of the numerical instability for the computer calculations.

The total scattering matrix for the whole system can be derived by an iteration process, using the set of equations 2.36.

The starting point of the iteration is:

$$\mathbf{S}(L,0) = \mathbf{1} \Leftrightarrow \begin{bmatrix}\mathbf{S}_{11}(L,0) & \mathbf{S}_{12}(L,0)\\ \mathbf{S}_{21}(L,0) & \mathbf{S}_{22}(L,0)\end{bmatrix} = \begin{bmatrix}\mathbf{1} & \mathbf{0}\\ \mathbf{0} & \mathbf{1}\end{bmatrix}$$

The iteration continues until the total matrix $\mathbf{S}(L,R) = \mathbf{S}(L,N+1)$ is finally obtained. The number of the slices N, that the nanostructure is divided, defines the number of iteration steps needed for the calculation of the total scattering matrix.

The boundary conditions of the system, that we study every time, allow to determine the expansion coefficients of the electromagnetic waves that are incident on the left or the right side of the nano-structure ($\left\{\mathbf{C}_L^{\alpha,+}\right\}$ and $\left\{\mathbf{C}_R^{\alpha,-}\right\}$, respectively). Finally, by inserting the total scattering matrix and the vectors $\mathbf{C}_L^+$ and $\mathbf{C}_R^-$, that contain the known expansion coefficients, to the eq.2.33 we are able to get the expansion coefficients of the expansion coefficients $\left\{\mathbf{C}_L^{\alpha,-}\right\}$ and $\left\{\mathbf{C}_R^{\alpha,+}\right\}$. Considering that the eigenvectors $\mathbf{d}_j^\alpha$ for each area have already been calculated from the eigenvalue equation (2.19),

it is clear that the total solution for the transverse components of the electric and magnetic field in the right or the left homogeneous area can be calculated.

In addition, it is possible to obtain the electric and magnetic field for any of the areas, that the system is divided into, by calculating the scattering matrices $\mathbf{S}(L, j)$ and $\mathbf{S}(j, R)$. The scattering matrix $\mathbf{S}(j, R)$ is calculated by an iteration process, using the equations 2.36. The iteration starts with $\mathbf{S}(j, j) = \mathbf{1}$ and continues until we reach to the $\mathbf{S}(j, N + 1) = \mathbf{S}(j, R)$. The expansion coefficients of the transverse components of the electric and magnetic field in the jth area of the system are given by the following equations [1][8] :

$$\mathbf{C}_j^+ = \left[\mathbf{1} - \mathbf{S}_{12}(L, j)\mathbf{S}_{21}(j, R)\right]^{-1} \left[\mathbf{S}_{11}(L, j)\mathbf{C}_L^+ + \mathbf{S}_{12}(L, j)\mathbf{S}_{22}(j, R)\mathbf{C}_R^-\right]$$
$$\mathbf{C}_j^- = \left[\mathbf{1} - \mathbf{S}_{21}(j, R)\mathbf{S}_{12}(L, j)\right]^{-1} \left[\mathbf{S}_{21}(j, R)\mathbf{S}_{11}(L, j)\mathbf{C}_L^+ + \mathbf{S}_{22}(j, R)\mathbf{C}_R^-\right]$$

The z components of the electric and the magnetic field can be calculated from the equations 2.3c and 2.4c, respectively, taking under consideration that the expressions of the x and y (transverse) components of the electric and magnetic field are known.

Finally, it is important to mention that the above described methods can be implemented in periodic structures, where a supercell can be applied. The methods work more efficiently when the number of the modes is limited and the structure consists of only few different slices[14].

2.3 System

The mathematical formalism, that has been described in the previous section, is a general method that can be implemented on any system. In this section the implementation of this formalism in the particular system of the nanostructure that is of interest for this work is presented.

2.3.1 Description of the system

The system, that we are interested in studying, consists of periodic vertical arrays of core-shell nanowires(Fig.2.2).

The core-shell nanowires are radially heterostructured nanowires. They consist of a core semiconductor material that is over-coated with a shell

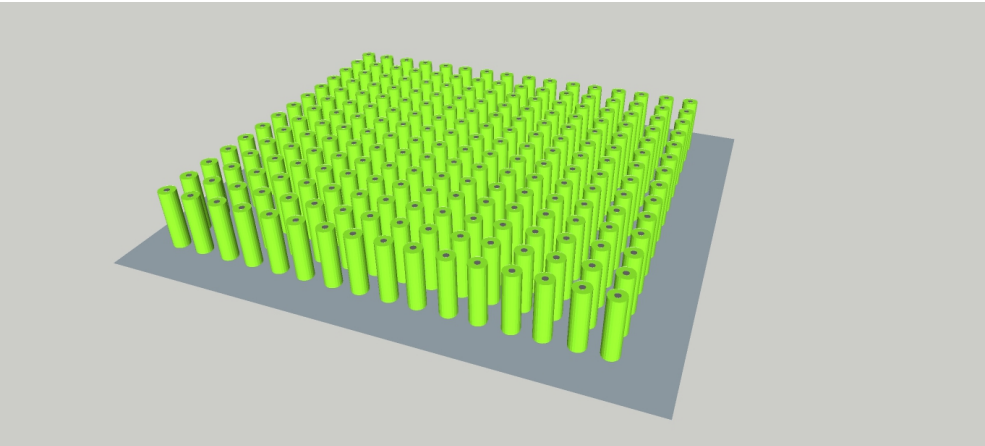

Figure 2.2: Nano-structure of periodic arrays of core-shell nanowires. The space above the nanowires and between them is filled with air and the substrate is a thick layer of SiO_2.

made by a different semiconductor material. It is important that the lattice constant of the core semiconductor matches with the lattice constant of the shell semiconductor material.

In the current work we are interested in core-shell nanowires with $InAs$ as the core material and InP as the shell material. The low energy bandgap semiconductor is used as the core material, while the semiconductor with the higher energy bandgap forms the shell of the nanowires. This decision is based on the absorption properties of the materials, since in this way the material that absorbs a larger spectrum of light frequencies is placed outside, while the less absorbing material is the core of the nanowire. Moreover, the electrical properties of the semiconductors are taken under consideration because by creating a heterostructure with the low energy bandgap material between two higher energy bandgap materials it is possible to collect the electrons, that are exited from the valence to the conduction band, when light is absorbed, in the core area.

The volume of the core material and the volume of the shell material are considered to be equal. This implies the following relation between the diameter of the shell and the diameter of the core (fig.2.4) :

$$D_{shell} = \sqrt{2} D_{core} \tag{2.37}$$

The periodic structure of the nanowire arrays is open on the top, assuming

that the space between the nanowires and above them is filled with air. The substrate is made of SiO_2 and it has thickness much higher than the height of the nanowires, so as to be considered as a semi-infinite homogeneous area.

The complex indices of refraction, that are used for the calculation of the relative permittivity, for the SiO_2 are taken from the Ref.[5] and for the semiconductors $(InP, InAs)$ we used the Ref.[3] as a source.

2.3.2 Implementation of the scattering matrix method for the system

The system is divided into three areas along the z direction(Fig.2.3). The first area is a semi-infinite homogeneous area of air. The second area is the slice of the nanowire arrays, where the permittivity is z-independent but it changes across the xy-plane according to the periodic system of the core-shell nanowires. The thickness of this slice is defined by the height of the nanowires, which is 2000nm. Finally, the third area is the substrate, that is a semi-infinite homogeneous area of SiO_2.

The structure of the nanowires is a periodic system, therefore the appropriate expansion basis $\{\phi_n(x,y)\}$ for the eigenmodes in eq.2.19 should satisfy the Bloch's theorem.

$$\phi_n(x,y) = \frac{1}{\sqrt{L_x}} e^{\left(\frac{2\pi}{L_x} n_x + k_x\right)x} \frac{1}{\sqrt{L_y}} e^{\left(\frac{2\pi}{L_y} n_y + k_y\right)y} \tag{2.38}$$

For the numerical calculations the n_x and n_y are limited inside the intervals $(-N_x, N_x)$ and $(-N_y, N_y)$,respectively. The limits N_x and N_y are integer numbers and they are very important because the accuracy of the calculations depends on how large values they get. However, the $\mathbf{T}_1^j$ and $\mathbf{T}_2^j$ matrices have dimensions of $2\left(2N_x+1\right)\left(2N_y+1\right) \times \left(2N_x+1\right)\left(2N_y+1\right)$ and if N_x and N_y will be increased very much the computational calculations will become really heavy. Therefore, we perform the calculations repeatedly with increased value of these limits until the results converge.

The matrix operators $\mathbf{T}_1^j$ and $\mathbf{T}_2^j$ are the projection of the operators $\hat{\mathbf{T}}_1^j$ and $\hat{\mathbf{T}}_2^j$ onto the orthonormal basis $\{\phi_n(x,y)\}$, as it is mentioned before. Consequently, the matrix elements of the sub-matrices that the operator matrix $\mathbf{T}_{1(2)}^j$ is constructed of, can be obtained from:

$$[\mathbf{T}_{1(2),ll'}^j]_{m,n} = < \phi_m | \hat{\mathbf{T}}_{1(2),ll'}^j | \phi_n >$$

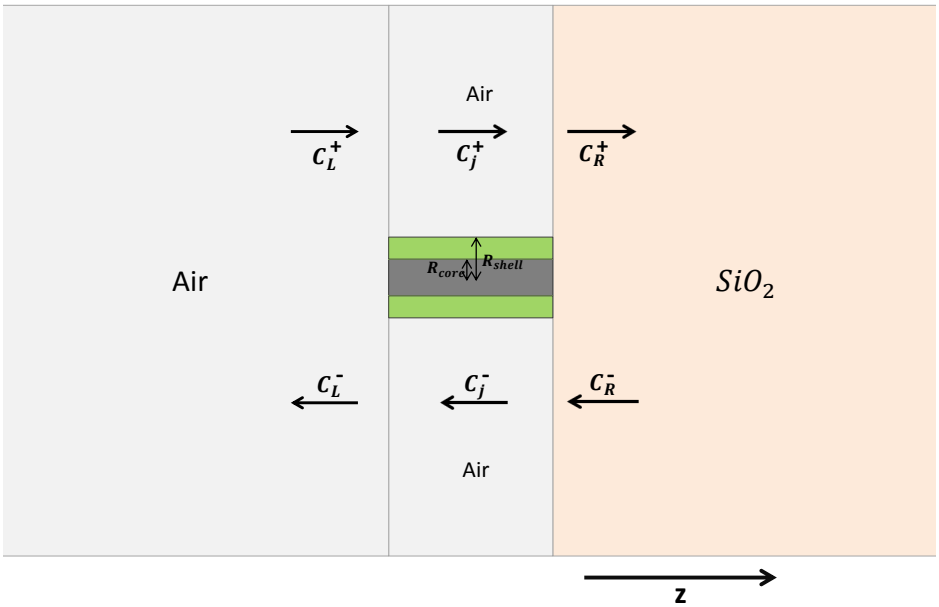

Figure 2.3: Vertical cross-section of the unit cell of the system along the z-direction, where the three areas that the system is divided are shown.

More specifically, the matrix elements of the sub-matrix $\mathbf{T}^j_{1,xx}$ could be calculated as follows:

$$[T^j_{1xx}]_{m,n} =< \phi_m|\frac{1}{i\omega}\frac{\partial}{\partial x}\frac{1}{\tilde{\epsilon}_j(x,y)}\frac{\partial}{\partial y}|\phi_n > \tag{2.39}$$

$$[T^j_{1xx}]_{m,n} =\iint \frac{1}{\sqrt{L_x}}e^{-i\frac{2\pi}{L_x}m_x x}\frac{1}{\sqrt{L_y}}e^{-i\frac{2\pi}{L_y}m_y y}\left(\frac{1}{i\omega}\frac{\partial}{\partial x}\frac{1}{\tilde{\epsilon}_j(x,y)}\frac{\partial}{\partial y}\right)\frac{1}{\sqrt{L_x}}e^{i\frac{2\pi}{L_x}n_x x}\frac{1}{\sqrt{L_y}}e^{i\frac{2\pi}{L_y}n_y y}dxdy$$

$$[T^j_{1xx}]_{m,n} =\iint \frac{1}{\sqrt{L_x}}e^{-i\frac{2\pi}{L_x}m_x x}\frac{1}{\sqrt{L_y}}e^{-i\frac{2\pi}{L_y}m_y y}\frac{1}{i\omega}\frac{\partial}{\partial x}\frac{1}{\tilde{\epsilon}_j(x,y)}\left(i\frac{2\pi}{L_y}n_y\right)\frac{1}{\sqrt{L_x}}e^{i\frac{2\pi}{L_x}n_x x}\frac{1}{\sqrt{L_y}}e^{i\frac{2\pi}{L_y}n_y y}dxdy$$

The permittivity is a periodic function and it is possible to be expanded in double Fourier series.

$$\tilde{\epsilon}_j(x,y) = \sum_{q_x}\sum_{q_y}\epsilon^j_{q_x,q_y}e^{i\frac{2\pi}{L_x}q_x x}e^{i\frac{2\pi}{L_y}q_y y}$$

Similarly, the inverse of the permittivity, that appears in the matrix element expression, can be expanded as follows:

$$\frac{1}{\widetilde{\epsilon}_j(x,y)} = \sum_{q_x}\sum_{q_y} \frac{1}{\epsilon^j_{q_x,q_y}} e^{i\frac{2\pi}{L_x}q_x x} e^{i\frac{2\pi}{L_y}q_y y} \tag{2.40}$$

where $\epsilon^j_{q_x,q_y}$ and $\frac{1}{\epsilon^j_{q_x,q_y}}$ are the expansion coefficients.

Thus, the matrix elements $[T^j_{1xx}]_{m,n}$ become :

$$[T^j_{1xx}]_{m,n} = \iint \frac{1}{\sqrt{L_x}} e^{-i\frac{2\pi}{L_x}m_x x} \frac{1}{\sqrt{L_y}} e^{-i\frac{2\pi}{L_y}m_y y} \frac{1}{i\omega}\frac{\partial}{\partial x}\left(\sum_{q_x}\sum_{q_y} \frac{1}{\epsilon^j_{q_x,q_y}} e^{i\frac{2\pi}{L_x}q_x x} e^{i\frac{2\pi}{L_y}q_y y}\right) \times \left(i\frac{2\pi}{L_y}n_y\right) \frac{1}{\sqrt{L_x}} e^{i\frac{2\pi}{L_x}n_x x} \frac{1}{\sqrt{L_y}} e^{i\frac{2\pi}{L_y}n_y y} dxdy$$

$$[T^j_{1xx}]_{m,n} = \frac{1}{i\omega}\frac{1}{L_x}\frac{1}{L_y} \iint e^{-i\frac{2\pi}{L_x}m_x x} e^{-i\frac{2\pi}{L_y}m_y y} \sum_{q_x}\sum_{q_y} \frac{1}{\epsilon^j_{q_x,q_y}} \left(i\frac{2\pi}{L_y}n_y\right)\left(\frac{\partial}{\partial x} e^{i\frac{2\pi}{L_x}(q_x+n_x)x} e^{i\frac{2\pi}{L_y}(q_y+n_y)y}\right) dxdy$$

$$[T^j_{1xx}]_{m,n} = \frac{1}{i\omega}\frac{1}{L_x}\frac{1}{L_y} \iint \sum_{q_x}\sum_{q_y} \frac{1}{\epsilon^j_{q_x,q_y}} \left(i\frac{2\pi}{L_y}n_y\right)\left(i\frac{2\pi}{L_x}(q_x+n_x)\right) e^{i\frac{2\pi}{L_x}(q_x+n_x-m_x)x} e^{i\frac{2\pi}{L_y}(q_y+n_y-m_y)y} dxdy$$

$$[T^j_{1xx}]_{m,n} = \frac{1}{i\omega} \sum_{q_x}\sum_{q_y} \frac{1}{\epsilon^j_{q_x,q_y}} \left(i\frac{2\pi}{L_y}n_y\right)\left(i\frac{2\pi}{L_x}(q_x+n_x)\right)\left(\frac{1}{L_x}\int e^{i\frac{2\pi}{L_x}(q_x+n_x-m_x)x} dx\right)\left(\frac{1}{L_y}\int e^{i\frac{2\pi}{L_y}(q_y+n_y-m_y)y} dy\right)$$

$$[T^j_{1xx}]_{m,n} = \frac{1}{i\omega}\left(i\frac{2\pi}{L_y}n_y\right) \sum_{q_x}\sum_{q_y} \left(i\frac{2\pi}{L_x}(q_x+n_x)\right) \frac{1}{\epsilon^j_{q_x q_y}} \delta(q_x+n_x-m_x)\delta(q_y+n_y-m_y)$$

Due to the Delta functions it becomes possible to remove the summations and substitute $q_x = m_x - n_x$ and $q_y = m_y - n_y$. Thus, we end up with:

$$[T^j_{1xx}]_{m,n} = \frac{1}{i\omega}\left(i\frac{2\pi}{L_y}n_y\right)\left(i\frac{2\pi}{L_x}m_x\right) \frac{1}{\epsilon^j_{(m_x-n_x),(m_y-n_y)}} \tag{2.41}$$

The expansion coefficients $\frac{1}{\epsilon^j_{(m_x-n_x),(m_y-n_y)}}$ could be obtained by applying an inverse transform to the Fourier series expansion:

$$\frac{1}{\epsilon^j_{(m_x-n_x),(m_y-n_y)}} = \frac{1}{L_x L_y}\int\int \frac{1}{\tilde{\epsilon}_j(x,y)} e^{-i\frac{2\pi}{L_x}(m_x-n_x)x} e^{-i\frac{2\pi}{L_y}(m_y-n_y)y} dxdy \tag{2.42}$$

This double integral can be calculated numerically. By discretizing the sides L_x and L_y of the unit cell of the periodic nano-structure (Fig.2.4) it becomes possible to convert the double integral into a double summation.

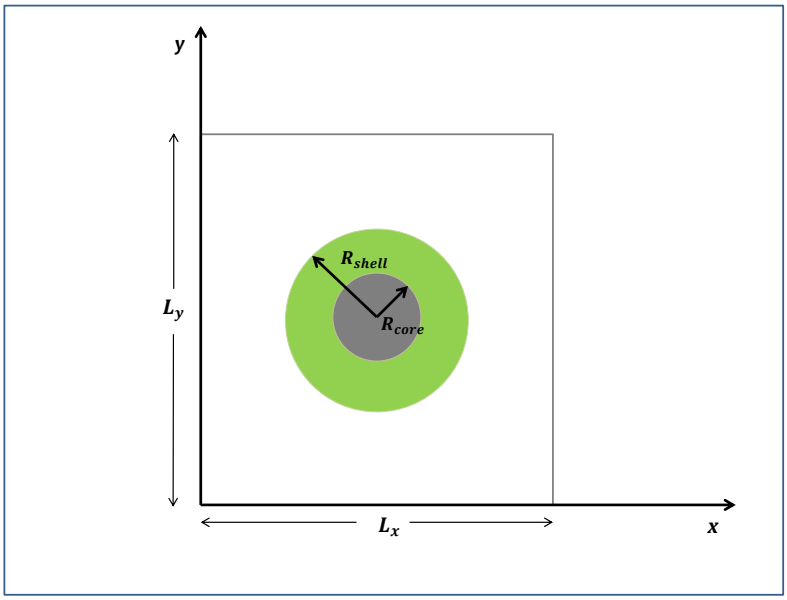

Figure 2.4: Horizontal cross-section of the unit cell of the periodic nanowire arrays. The L_x and L_y define the period of the system.

The lengths L_x and L_y are divided into N discrete intervals and each of these intervals has length of:

$$dx = \frac{L_x}{N} \quad and \quad dy = \frac{L_y}{N}$$

Moreover, the x and y coordinates should be written as:

$$x = kdx = k\frac{L_x}{N}$$

$$y = ldy = l\frac{L_y}{N}$$

where k and l are the indices of double summation.

In addition, by converting the double integral into a double summation and taking under consideration the structure of the unit shell, that reflects the different values of the permittivity of the system across the xy-plane, the eq.2.42 can be written as:

$$\begin{aligned}\frac{1}{\epsilon^j_{(m_x-n_x),(m_y-n_y)}} = &\frac{1}{L_xL_y}\sum_{l=0}^{N}\sum_{k=0}^{N}\frac{1}{\epsilon_{air}}e^{i\frac{2\pi}{L_x}(m_x-n_x)k\frac{L_x}{N}}e^{i\frac{2\pi}{L_y}(m_y-n_y)l\frac{L_y}{N}}\frac{L_x}{N}\frac{L_y}{N}+\\ &+\frac{1}{L_xL_y}\sum_{l=l_1}^{l_2}\sum_{k=k_1}^{k_2}\left(\frac{1}{\epsilon_{shell}}-\frac{1}{\epsilon_{air}}\right)e^{i\frac{2\pi}{L_x}(m_x-n_x)k\frac{L_x}{N}}e^{i\frac{2\pi}{L_y}(m_y-n_y)l\frac{L_y}{N}}\frac{L_x}{N}\frac{L_y}{N}+\\ &+\frac{1}{L_xL_y}\sum_{l=l'_1}^{l'_2}\sum_{k=k'_1}^{k'_2}\left(\frac{1}{\epsilon_{core}}-\frac{1}{\epsilon_{shell}}\right)e^{i\frac{2\pi}{L_x}(m_x-n_x)k\frac{L_x}{N}}e^{i\frac{2\pi}{L_y}(m_y-n_y)l\frac{L_y}{N}}\frac{L_x}{N}\frac{L_y}{N}\end{aligned}$$

$$\begin{aligned}\frac{1}{\epsilon^j_{(m_x-n_x),(m_y-n_y)}} = &\frac{1}{N^2}\sum_{l=0}^{N}\sum_{k=0}^{N}\frac{1}{\epsilon_{air}}e^{i\frac{2\pi}{N}(m_x-n_x)k}e^{i\frac{2\pi}{N}(m_y-n_y)l}+\\ &+\frac{1}{N^2}\sum_{l=l_1}^{l_2}\sum_{k=k_1}^{k_2}\left(\frac{1}{\epsilon_{shell}}-\frac{1}{\epsilon_{air}}\right)e^{i\frac{2\pi}{N}(m_x-n_x)k}e^{i\frac{2\pi}{N}(m_y-n_y)l}+\\ &+\frac{1}{N^2}\sum_{l=l'_1}^{l'_2}\sum_{k=k'_1}^{k'_2}\left(\frac{1}{\epsilon_{core}}-\frac{1}{\epsilon_{shell}}\right)e^{i\frac{2\pi}{N}(m_x-n_x)k}e^{i\frac{2\pi}{N}(m_y-n_y)l}\end{aligned}$$

Here ϵ_{shell} and ϵ_{core} are the values of the permittivity of the shell and core semiconductor materials, respectively. The limits k_1, k_2 and l_1, l_2 define the external circle of the shell and the limits k'_1, k'_2 and l'_1, l'_2 define the external circle of the core.

These limits can be calculated by:

$$l_1 = \frac{\frac{L_y}{2} - R_{shell}}{L_y} N$$

$$l_2 = \frac{\frac{L_y}{2} + R_{shell}}{L_y} N$$

$$k_1 = \frac{\frac{L_x}{2}}{L_x} N - \sqrt{\left(\frac{R_{shell}}{L_x} N\right)^2 - \left(l - \frac{\frac{L_x}{2}}{L_x} N\right)^2}$$

$$k_2 = \frac{\frac{L_x}{2}}{L_x} N + \sqrt{\left(\frac{R_{shell}}{L_x} N\right)^2 - \left(l - \frac{\frac{L_x}{2}}{L_x} N\right)^2}$$

Similarly, for the core:

$$l'_1 = \frac{\frac{L_y}{2} - R_{core}}{L_y} N$$

$$l'_2 = \frac{\frac{L_y}{2} + R_{core}}{L_y} N$$

$$k'_1 = \frac{\frac{L_x}{2}}{L_x} N - \sqrt{\left(\frac{R_{core}}{L_x} N\right)^2 - \left(l - \frac{\frac{L_x}{2}}{L_x} N\right)^2}$$

$$k'_2 = \frac{\frac{L_x}{2}}{L_x} N + \sqrt{\left(\frac{R_{core}}{L_x} N\right)^2 - \left(l - \frac{\frac{L_x}{2}}{L_x} N\right)^2}$$

By following the same derivation the rest of the matrix elements could be calculated. Hence, the following matrix elements can be obtained.

$$
\begin{aligned}
[T^j_{1xx}]_{m,n} =& \frac{1}{i\omega}\left(i\frac{2\pi}{L_y}n_y\right)\left(i\frac{2\pi}{L_x}m_x\right)\frac{1}{\epsilon^j_{(m_x-n_x),(m_y-n_y)}}\\
[T^j_{1xy}]_{m,n} =& i\omega\tilde{\mu}_j(x,y)\delta(n_x-m_x)\delta(n_y-m_y)+\left(-\frac{1}{i\omega}\right)\left(i\frac{2\pi}{L_x}n_x\right)\left(i\frac{2\pi}{L_x}m_x\right)\frac{1}{\epsilon^j_{(m_x-n_x),(m_y-n_y)}}\\
[T^j_{1yx}]_{m,n} =& -i\omega\tilde{\mu}_j(x,y)\delta(n_x-m_x)\delta(n_y-m_y)+\left(\frac{1}{i\omega}\right)\left(i\frac{2\pi}{L_y}n_y\right)\left(i\frac{2\pi}{L_y}m_y\right)\frac{1}{\epsilon^j_{(m_x-n_x),(m_y-n_y)}}\\
[T^j_{1yy}]_{m,n} =& -\frac{1}{i\omega}\left(i\frac{2\pi}{L_x}n_x\right)\left(i\frac{2\pi}{L_y}m_y\right)\frac{1}{\epsilon^j_{(m_x-n_x),(m_y-n_y)}}
\end{aligned}
$$

Finally, by using the same derivation we obtain the matrix elements of the sub-matrices of the operator matrix $\mathbf{T}^j_2$:

$$
\begin{aligned}
[T^j_{2xx}]_{m,n} =& -\frac{1}{i\omega\tilde{\mu}_j(x,y)}\left(i\frac{2\pi}{L_y}n_y\right)\left(i\frac{2\pi}{L_x}n_x\right)\delta(n_x-m_x)\delta(n_y-m_y)\\
[T^j_{2xy}]_{m,n} =& -i\omega\epsilon^j_{(m_x-n_x),(m_y-n_y)}+\frac{1}{i\omega\tilde{\mu}_j(x,y)}\left(i\frac{2\pi}{L_x}n_x\right)\left(i\frac{2\pi}{L_x}n_x\right)\delta(n_x-m_x)\delta(n_y-m_y)\\
[T^j_{2yx}]_{m,n} =& i\omega\epsilon^j_{(m_x-n_x),(m_y-n_y)}-\frac{1}{i\omega\tilde{\mu}_j(x,y)}\left(i\frac{2\pi}{L_y}n_y\right)\left(i\frac{2\pi}{L_y}n_y\right)\delta(n_x-m_x)\delta(n_y-m_y)\\
[T^j_{2yy}]_{m,n} =& \frac{1}{i\omega\tilde{\mu}_j(x,y)}\left(i\frac{2\pi}{L_y}n_y\right)\left(i\frac{2\pi}{L_x}n_x\right)\delta(n_x-m_x)\delta(n_y-m_y)
\end{aligned}
$$

where the expansion coefficients $\epsilon^j_{(m_x-n_x),(m_y-n_y)}$ are calculated in the same way as the expansion coefficients $\frac{1}{\epsilon^j_{(m_x-n_x),(m_y-n_y)}}$ are calculated.

The $\mathbf{T}^j_1$ and $\mathbf{T}^j_2$ are non-Hermitian, non-symmetric complex matrices in the case of the nanowire area, where the permittivity is altered across xy-plane. On the other hand, for the homogeneous areas on the left and the right side of the nanowire area, where the permittivity has constant value everywhere, the matrix elements of the sub-matrices, that $\mathbf{T}^j_1$ and $\mathbf{T}^j_2$ are

constructed of, are diagonal and their matrix elements can be calculated by:

$$
\begin{aligned}
[T^j_{1xx}]_{m,n} =& \frac{1}{i\omega}\left(i\frac{2\pi}{L_y}n_y\right)\left(i\frac{2\pi}{L_x}m_x\right)\left(\frac{1}{\epsilon^j}\right)\delta(n_x-m_x)\delta(n_y-m_y)\\
[T^j_{1xy}]_{m,n} =& i\omega\tilde{\mu}_j(x,y)\delta(n_x-m_x)\delta(n_y-m_y)+\left(-\frac{1}{i\omega}\right)\left(i\frac{2\pi}{L_x}n_x\right)\left(i\frac{2\pi}{L_x}m_x\right)\left(\frac{1}{\epsilon^j}\right)\delta(n_x-m_x)\delta(n_y-m_y)\\
[T^j_{1yx}]_{m,n} =& -i\omega\tilde{\mu}_j(x,y)\delta(n_x-m_x)\delta(n_y-m_y)+\left(\frac{1}{i\omega}\right)\left(i\frac{2\pi}{L_y}n_y\right)\left(i\frac{2\pi}{L_y}m_y\right)\left(\frac{1}{\epsilon^j}\right)\delta(n_x-m_x)\delta(n_y-m_y)\\
[T^j_{1yy}]_{m,n} =& -\frac{1}{i\omega}\left(i\frac{2\pi}{L_x}n_x\right)\left(i\frac{2\pi}{L_y}m_y\right)\left(\frac{1}{\epsilon^j}\right)\delta(n_x-m_x)\delta(n_y-m_y)
\end{aligned}
$$

and

$$
\begin{aligned}
[T^j_{2xx}]_{m,n} =& -\frac{1}{i\omega\tilde{\mu}_j(x,y)}\left(i\frac{2\pi}{L_y}n_y\right)\left(i\frac{2\pi}{L_x}n_x\right)\delta(n_x-m_x)\delta(n_y-m_y)\\
[T^j_{2xy}]_{m,n} =& -i\omega\epsilon^j\delta(n_x-m_x)\delta(n_y-m_y)+\frac{1}{i\omega\tilde{\mu}_j(x,y)}\left(i\frac{2\pi}{L_x}n_x\right)\left(i\frac{2\pi}{L_x}n_x\right)\delta(n_x-m_x)\delta(n_y-m_y)\\
[T^j_{2yx}]_{m,n} =& i\omega\epsilon^j\delta(n_x-m_x)\delta(n_y-m_y)-\frac{1}{i\omega\tilde{\mu}_j(x,y)}\left(i\frac{2\pi}{L_y}n_y\right)\left(i\frac{2\pi}{L_y}n_y\right)\delta(n_x-m_x)\delta(n_y-m_y)\\
[T^j_{2yy}]_{m,n} =& \frac{1}{i\omega\tilde{\mu}_j(x,y)}\left(i\frac{2\pi}{L_y}n_y\right)\left(i\frac{2\pi}{L_x}n_x\right)\delta(n_x-m_x)\delta(n_y-m_y)
\end{aligned}
$$

2.3.3 Boundary conditions of the system

The polarization and the angle of incidence of the incoming light set the boundary conditions of the system. We consider that the light is incident on the left side of the structure, consequently the expansion coefficients of the electromagnetic waves for the right side incident light (Fig.2.3) should be zero.

$$\mathbf{C}_R^- = \mathbf{0}$$

In addition, the incident light is treated as a plane wave that impinges normally towards the top surface of the nanowires (normally to the xy-plane), with direction of propagation the z-direction. As a result the wave vector $\mathbf{k} = (k_x, k_y, k_z)$ should have:

$$k_x = k_y = 0 \text{ and } k_z \neq 0$$

Finally, the incident light is x-polarized light and it is possible to set:

$$\mathbf{E}_L(x, y, z_L) = \hat{\mathbf{e}}_x$$

For y-polarized incident light the results would not be different due to the symmetry of the system. The case of circular (or elliptical) polarized incident light will have a different outcome, but it is not going to be studied in the current thesis work.

2.4 Absorptance

The scattering matrix method allows us to solve the Maxwell equations for the periodic structure of the nanowire arrays and calculate the electric and magnetic field inside the different areas of the system. In addition, we are in the position to calculate the $Transmittance$ and the $Reflectance$ of light in different wavelengths of the incoming light, but also for different geometrical parameters of the nano-structure.

In fact, we alter the values of the shell diameter, which results in varying the core diameter, because these two variables are related as the eq.2.37 shows. For each value of the shell diameter we calculate the $Transmittance$ and the $Reflectance$ for different wavelengths of the incoming light, starting from 400nm to 700nm.

Moreover, the *Absorptance* for each wavelength can be extracted from the $Transmittance$ and $Reflectance$, using the simple relation:

$$\textit{Absorptance} = 1 - \textit{Transmittance} - \textit{Reflectance} \tag{2.49}$$

Firstly, we need to calculate the energy flow through the xy-surface along the z direction for the left and right homogeneous areas. This energy flow can be calculated from the time averaged Poynting vector:

$$I_{L(R)} = \int \langle \mathbf{S} \rangle \, \hat{\mathbf{n}} \, dA \tag{2.50}$$

where A is the surface of the xy-plane and the $\hat{\mathbf{n}}$ is the surface normal vector.

The time averaged Poynting vector is:

$$\langle \mathbf{S} \rangle = \frac{1}{T} \int_0^T \mathbf{S} dt = \frac{1}{T} \int_0^T (\mathbf{E}_{tot} \times \mathbf{H}_{tot})\, dt$$

where T is the period of the electromagnetic wave. Taking under consideration that the electromagnetic fields have a harmonic dependence on time the total electric and magnetic fields can be written as:

$$\mathbf{E}_{tot} = Re\{\mathbf{E}e^{-i\omega t}\} = \frac{1}{2}\left(\mathbf{E}e^{-i\omega t} + (\mathbf{E}e^{-i\omega t})^*\right) \tag{2.51a}$$

$$\mathbf{H}_{tot} = Re\{\mathbf{H}e^{-i\omega t}\} = \frac{1}{2}\left(\mathbf{H}e^{-i\omega t} + (\mathbf{H}e^{-i\omega t})^*\right) \tag{2.51b}$$

The $\mathbf{E}_{tot}$ and $\mathbf{H}_{tot}$ have real values, while the time-independent $\mathbf{E}$ and $\mathbf{H}$ take complex values.

By introducing the complex expression of the electric and magnetic fields, we get:

$$\begin{aligned}\langle \mathbf{S} \rangle =& \frac{1}{4T} \int_0^T \left(\mathbf{E}e^{-i\omega t} + \mathbf{E}^* e^{i\omega t}\right) \times \left(\mathbf{H}e^{-i\omega t} + \mathbf{H}^* e^{i\omega t}\right) dt = \\ =& \frac{1}{4T} \int_0^T \left((\mathbf{E} \times \mathbf{H})e^{-2i\omega t} + \mathbf{E}^* \times \mathbf{H} + \mathbf{E} \times \mathbf{H}^* + (\mathbf{E}^* \times \mathbf{H}^*)e^{2i\omega t}\right)\end{aligned}$$

Calculating the integrals as follows:

$$\begin{cases} \int_0^T (\mathbf{E} \times \mathbf{H})\, e^{-2i\omega t} dt = \int_0^T (\mathbf{E}^* \times \mathbf{H}^*)\, e^{2i\omega t} dt = 0 \\ \frac{1}{T} \int_0^T (\mathbf{E}^* \times \mathbf{H})\, dt = \mathbf{E}^* \times \mathbf{H} \\ \frac{1}{T} \int_0^T (\mathbf{E} \times \mathbf{H}^*)\, dt = \mathbf{E} \times \mathbf{H}^* \end{cases}$$

the time averaged Poynting vector can be written as:

$$\langle \mathbf{S} \rangle = \frac{1}{4} (\mathbf{E}^* \times \mathbf{H} + \mathbf{E} \times \mathbf{H}^*) = \frac{1}{2} Re\, (\mathbf{E} \times \mathbf{H}^*)$$

By substituting that in the eq.2.50, we get:

$$I_{L(R)} = \int \langle S_z \rangle \, dxdy \tag{2.53}$$

It is very useful, at this point, to categorise the propagating modes of light into different groups. When light propagates inside the homogeneous areas, the light polarization allows us to distinguish the light into three different types of eigenmodes:

- the **transverse electric** (TE) modes, where $\tilde{E}_z^\alpha(x, y) = 0$ for every x and y,
- the **transverse magnetic** (TM) modes, where $\tilde{H}_z^\alpha(x, y) = 0$ for every x and y,
- and the **transverse electromagnetic** (TEM) modes, where $\tilde{E}_z^\alpha(x, y) = 0$ and $\tilde{H}_z^\alpha(x, y) = 0$ for every x and y.

The eigenmodes are orthonormalized, hence the eq.2.53 can be solved for each type of eigenmode.[1]

$$I_{L(R)} = \sum_{\alpha}^{Re} \gamma^\alpha_{L(R),M_\alpha^{L(R)}} \left[|C^{+,\alpha}_{L(R)}|^2 - |C^{-,\alpha}_{L(R)}|^2 \right] \tag{2.54}$$

where $M_\alpha^{L(R)}$ denotes the type of mode:

$$\gamma^\alpha_{L(R),TE} = \frac{k^\alpha_{L(R)}}{2\omega\tilde{\mu}_{L(R)}} \ , \ \text{for TE modes}$$
$$\gamma^\alpha_{L(R),TM} = \frac{\omega\tilde{\epsilon}_{L(R)}}{2k^\alpha_{L(R)}} \ , \quad \text{for TM modes}$$
$$\gamma^\alpha_{L(R),TEM} = \frac{k^\alpha_{L(R)}}{2\omega\tilde{\mu}_{L(R)}} \ , \quad \text{for TEM modes}$$

The summation should include only the modes that have real values for the wave vectors $k^\alpha_{L(R)}$.

The energy flow in each area could be calculated from the previous equations, but also the direction of the energy flows could be distinguished. Thus, it becomes possible to calculate the energy flow for the incident, transmitted and reflected light, taking under consideration that the light is incident only on the left side.

$$I_{incident} = \sum_{\alpha}^{Re} \gamma^{\alpha}_{L,M^L_\alpha} |C^{+,\alpha}_L|^2$$

$$I_{transmitted} = \sum_{\alpha}^{Re} \gamma^{\alpha}_{R,M^R_\alpha} |C^{+,\alpha}_R|^2$$

$$I_{reflected} = \sum_{\alpha}^{Re} \gamma^{\alpha}_{L,M^L_\alpha} |C^{-,\alpha}_L|^2$$

Once these values are obtained, the $Transmittance$ and the $Reflectance$ can be calculated by:

$$T = \frac{I_{transmitted}}{I_{incident}} \tag{2.57}$$

$$R = \frac{I_{reflected}}{I_{incident}} \tag{2.58}$$

2.5 Computer calculations and programming

It is obvious from the amount of data that needed to be handled for the numerical calculations that the solutions can be obtained only by using a computer program. The algorithm, that is created in order to implement the mathematical derivation, has been developed with C++ programming language. For the linear algebraic operations the algorithm uses the *Eigen* 3.2.1 library. *Eigen* is a library for C++ with template headers for linear algebra, matrix and vector operations, numerical solvers and related algorithms.

The algorithm was initially designed for the system that has already been studied in the paper of the Ref.[1] by N.Anttu and H.Q.Xu, in order to recreate the results of the paper. By comparing the results that our algorithm

produced with the results of the paper, it became possible to test the efficiency of the program and verify that it works properly. The next step is to make a few changes to the code in order to adjust it to the system of the core-shell nanowires.

As it was mentioned before, the size of the expansion basis defines the precision of the results. When the value of the parameter N_x or N_y, which sets the size of the expansion basis, increases the results become more accurate, but at the same time the calculations become heavier and the computational time increases significantly. The reason that the calculations slow down, when a large basis is used, is that the size of the matrices is directly connected with the size of the basis. In addition, the matrix, in the eigenvalue equation 2.19, is a non-Hermitian, non-symmetric complex matrix, which means that the eigensolver, needed to be used, is a general eigensolver and it cannot use any of the algebraic properties that speed up the calculations. Thus, the real challenge of this venture is to create an algorithm that is optimized to handle such a large amount of data requiring as short computational time as possible.

The calculations are performed with gradually increased basis size and the objective is to find the basis size where the results converge. The largest basis size that we are able to use is: $N_x = N_y = 27$. By using an expansion basis with these limits, the error of the calculations is minimized and the results are very precise, but the computation time is not acceptable for the limited time of this thesis work. Thus, considering the time limitations, it is decided that a basis with a smaller size should be used in order to collect sufficient amount of data and at the same time by calculating the error to put the results in the right perspective and give a clear picture of the conclusions.

The basis size, that is used, is $N_x = N_y = 21$ and a typical calculation time for a certain wavelength of incoming light is approximately 3 hours. The error is calculated by comparing the results from this basis with the results obtained with basis size $N_x = N_y = 27$. It will be clear from the next chapter of the results that the basis, that is used, allows us to draw important conclusions regarding the absorbing behaviour of the system and the results are in agreement with the theory and with previous similar periodic systems of nanowire arrays. Moreover, it is very important to present the error and explain the error characteristics in a proper manner, in order to avoid any misinterpretation of the results.

Chapter 3

Results

3.1 Transmittance, Reflectance and Absorptance

The previous theoretical derivation is implemented in the system that has been described. Initially, the period of the nanowire arrays is constant, with value $L_x = L_y = 500$nm. The $Transmittance$ and the $Reflectance$ of the system is calculated for a certain shell diameter of the nanowires, for different frequencies of the incoming light. The light wavelength is varied between 400nm and 700nm and the two properties are calculated. From the $Transmittance$ and the $Reflectance$ it is straightforward to calculate the *Absorptance*(eq.2.49).

We repeat the calculations for different shell diameters. The shell diameter is changing, starting from 100nm until it reaches the value of the period of the system. As mentioned before, this change of the shell diameter results in a change of the diameter of the core (eq.2.37), in order to have the same volume of the shell and the core of the nanowires. Finally, the $Transmittance$, the $Reflectance$ and the *Absorptance* for different shell diameters and different wavelengths of incoming light is plotted.

The *Absorptance* diagram for a system with period $L_x = L_y = 500$nm is presented in fig.3.1. The *Absorptance* is generally very high for this system and this is because of the combination of the two materials with different energy band gaps in the core - shell nanowires. The other important observation that is worth-mentioning is that there are certain areas in this plot where the *Absorptance* reaches to its peak values. The *Absorptance* in these

areas has peak values higher than 0.98. A more profound study of these areas is necessary, in order to find the mechanisms that can explain this absorbing behaviour.

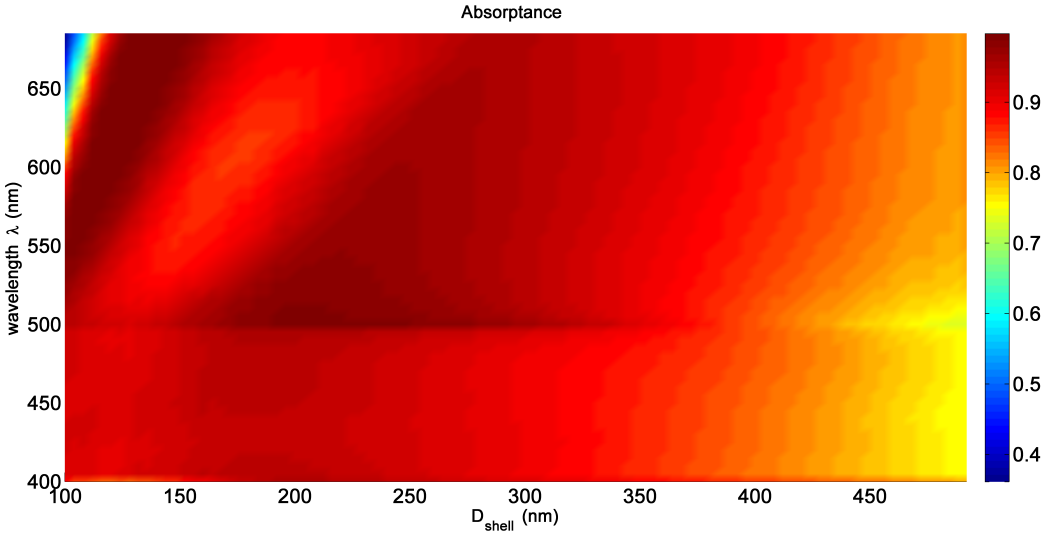

Figure 3.1: *Absorptance* spectrum for different shell diameters. The wavelength of the incoming light is varied between 400nm and 700nm. The period of the nanowire arrays is $L_x = L_y = 500$nm

The first area, where peak values of the *Absorptance* are observed, is the area where the shell diameter of the nanowires is between 100nm and 170nm. As the diameter of the shell increases the peak is moving to longer wavelengths of incoming light. The relation between the shell diameter and the wavelength of the incoming light, where the *Absorptance* peak is observed, is almost linear. The peak in the *Absorptance* for the shell diameter $D_{shell} = 100$nm corresponds to incoming light with wavelength $\lambda \simeq 550$nm and it is not a sharp peak. As it can be seen in fig.3.2, the peak for diameter $D_{shell} = 100$nm is broaden and the highest value of the *Absorptance* is 0.988. This *Absorptance* peak corresponds to wavelength $\lambda = 500$nm for the incoming light. Similar behaviour can be observed for all the shell diameters between 100nm and 172nm and it is obvious from the fig.3.2 that the peak is moving to longer wavelengths of the incoming light, as the shell diameter increases.

The width of this area is related to the fact that the peaks in *Absorptance* for every shell diameter are broadened. It is also clear from our data that

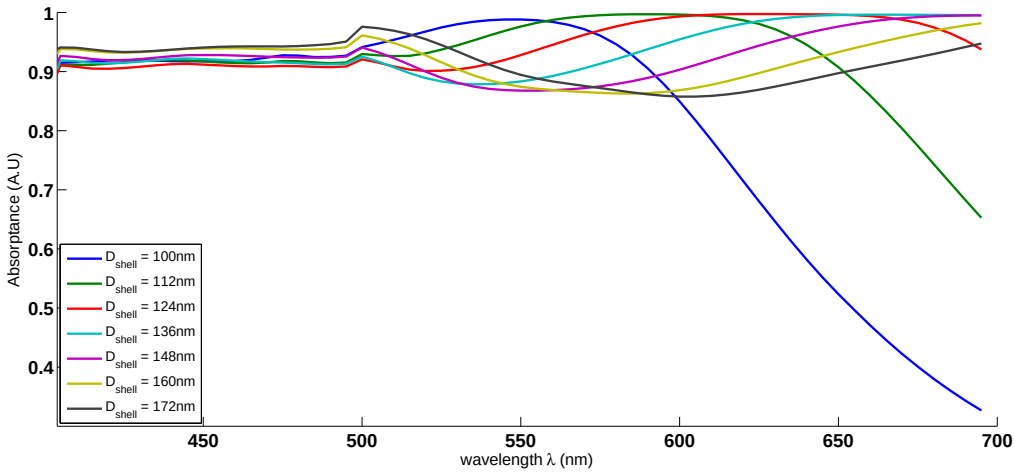

Figure 3.2: The plot of the *Absorptance* with wavelength of incoming light for different value of the shell diameter. The period of the nanowire arrays is $L_x = L_y = 500$nm.

this area of the maximum *Absorptance* continues to longer wavelengths of incoming light as the shell diameter increases above the 170nm, however, this can not be seen in the fig.3.1 because the spectrum of the incoming light taken under consideration, is between 400nm and 700nm ($400nm \leq \lambda \leq 700nm$).

The high value for the *Absorptance* in this area can be explained if we consider that certain wave modes of light can be trapped inside the nanowires.

Generally, depending on the value of the wave vector k the solutions of the Maxwell equations can be separated into two basic categories of modes[4],[13]:

1. the *guided modes*, that propagate inside the waveguide without loosing energy. These modes correspond to **real** and **discrete** values of k. They cannot be observed in the nanowires of the system that is studied here.

2. the *radiation modes*, which can be further divided into the following sub-categories:

   - if k takes **complex** and **discrete** values, then the modes are called *leaky modes* or guided pseudo-modes. These modes propagate like guided modes, but they are attenuated along the z-direction because the presence of the imaginary part of k at the exponential ($e^{ikz} = e^{ik_{real}z}e^{-k_{imag}z}$) results in a decrease of the amplitude.

- if k takes a **continuum** of **real** values, the modes attenuate very rapidly and if k takes a **continuum** of **purely imaginary** values, the modes are evanescent modes along the z-direction and they do not propagate inside the waveguide, since k does not have a real part. These last two cases where k takes a continuum of value cannot be observed in our system, as well.

In conclusion, for certain values of the shell diameter we can explain the high *Absorptance* by the excitation of these *leaky modes*. The *leaky modes* are excited when the shell diameter combines with certain wavelengths of incoming light and results in trapping the light. Hence, certain resonant states of standing light waves, that we call modes, are formed inside the nanowires. It is obvious that by increasing the diameter of the shell, the modes that are trapped inside the nanowires correspond to incoming light with longer wavelengths. This can explain why the peak of the *Absorptance* moves to longer wavelengths, when the shell diameter is increased. The existence of these modes will be very clear later on in this thesis, when the electric field distributions along the cross-section of the nanowires will be presented.

The second area with high *Absorptance* is the area that is confined between the $D_{shell} \simeq 130$nm and $D_{shell} \simeq 340$nm and starts with a wavelength of incoming light $\lambda = 500nm$ and continues to longer wavelengths of incoming light, forming a triangular area of high *Absorptance* (fig.3.1). The *Absorptance* is gradually decreased, as the wavelength increases. The maximum values of the *Absorptance* in this area are observed for $\lambda = 500$nm and they are higher than 0.97. Especially, for shell diameter between 200nm and 230nm ($200nm \leq D_{shell} \leq 230nm$) and wavelength $\lambda = 500$nm the *Absorptance* is slightly higher than 0.99. This peak can also be seen in figures 3.2 and 3.3, where it is clear that the peak is growing as the shell diameter takes larger values. When the shell diameter increases above the value of the 230nm the peak values in *Absorptance* become smaller (fig.3.3) and eventually the peak disappears.

The fact that the wavelength of the light, when the highest *Absorptance* occurs, coincides with the period of the nanowire arrays ($L_x = L_y = 500$nm) indicates that this maximum in *Absorptance* is probably the result of coupling between different nanowires' electric fields. More specifically, the electric field of the light, that *leaks out* of a nanowire or is reflected upon its surface, interferes with the electric field that comes from the nanowires (again

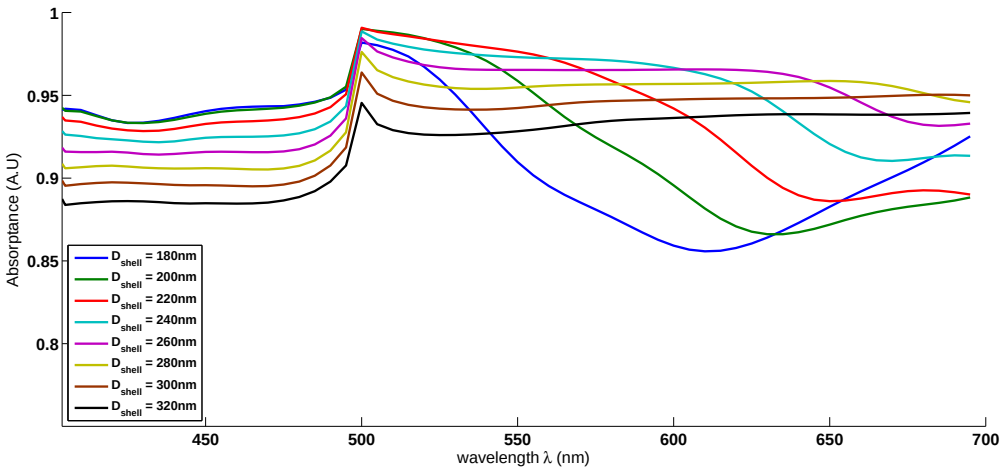

Figure 3.3: The plot of the *Absorptance* with wavelength of incoming light for different value of the shell diameter. The period of the nanowire arrays is $L_x = L_y = 500$nm.

because of the light that escapes or is reflected upon the surface) that exist in close vicinity. For incoming light with a wavelength equal to the period of the structure, the structure acts as a Bragg grating and the light is trapped inside until it is absorbed. This phenomenon is weak when the diameter of the nanowires is short because the coupling is weak but it becomes more obvious as the shell diameter increases.

Finally, for large shell diameters it is clear from the diagram in fig.3.1 that the *Absorptance* becomes weaker. This is because the nanowires cover almost completely the whole surface of the unit cell and the material behaves similarly with the bulk material. It can be seen from the $Reflectance$ diagram in fig.3.4, the system for large shell diameters is more reflective, as it is expected.

To sum up, two very important phenomena of light interaction with nanomaterials can be observed here. The first is the excitation of the light propagating modes at the individual nanowires, that results into high values of *Absorptance* and the second is the interference between the electromagnetic fields of the propagation modes that are excited inside different individual nanowires. This coupling can be observed not only between neighbouring nanowires but also between nanowires that are relatively further apart, al-

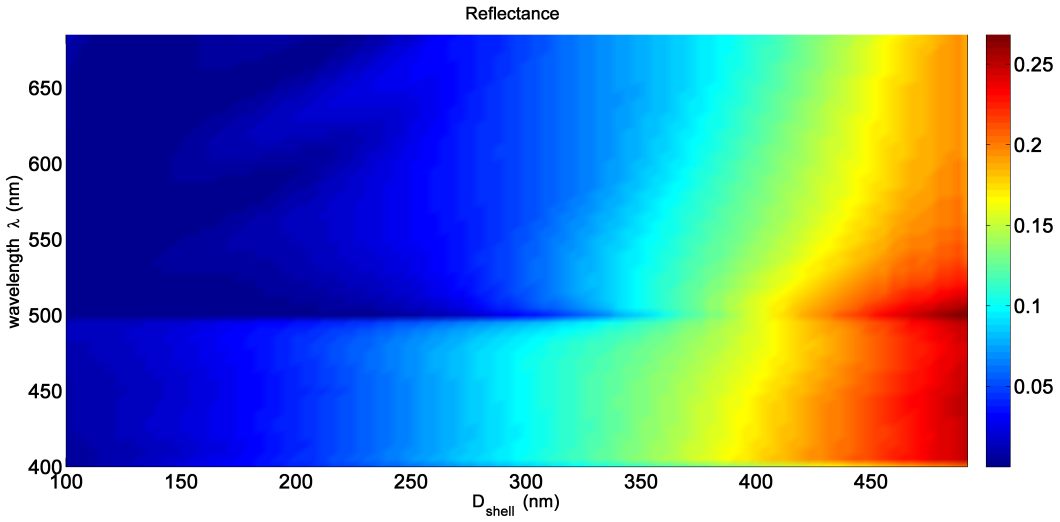

Figure 3.4: *Reflectance* spectrum for different shell diameters. The wavelength of the incoming light is varied between 400nm and 700nm. The period of the nanowire arrays is $L_x = L_y = 500$nm.

beit, the results are weaker and less obvious.

Additionally, in order to verify the above mentioned observations we repeat the calculations for different periods of the system. The calculations are performed for periods $L_x = L_y = 410$nm and $L_x = L_y = 600$nm. We choose to do the calculations for 410nm, instead of 400nm, because in this way a possible peak that appears at wavelength equal to the period will be more clearly visible. The results are plotted and shown in figures 3.5 and 3.6.

By comparing the plots in figures 3.5, 3.1 and 3.6 - that correspond to periods 410nm, 500nm and 600nm, respectively - it is safe to say that we observe the same pattern. The two areas, with high values of *Absorptance*, can be seen very clearly in all the diagrams.

The area, where the high *Absorptance* is coming from the excitation of the light propagation modes from individual nanowires, has the same shape and form, in all three diagrams. The high *Absorptance* in this area does not depend on the period of the system, since it is a result of the fact that the light is trapped inside each individual nanowire. Thus, it is reasonable that the system exhibits almost identical absorbing behaviour for different periods, at these values of shell diameter and wavelength, that correspond to the above mentioned area in the plots. The plot in fig.3.7 supports the

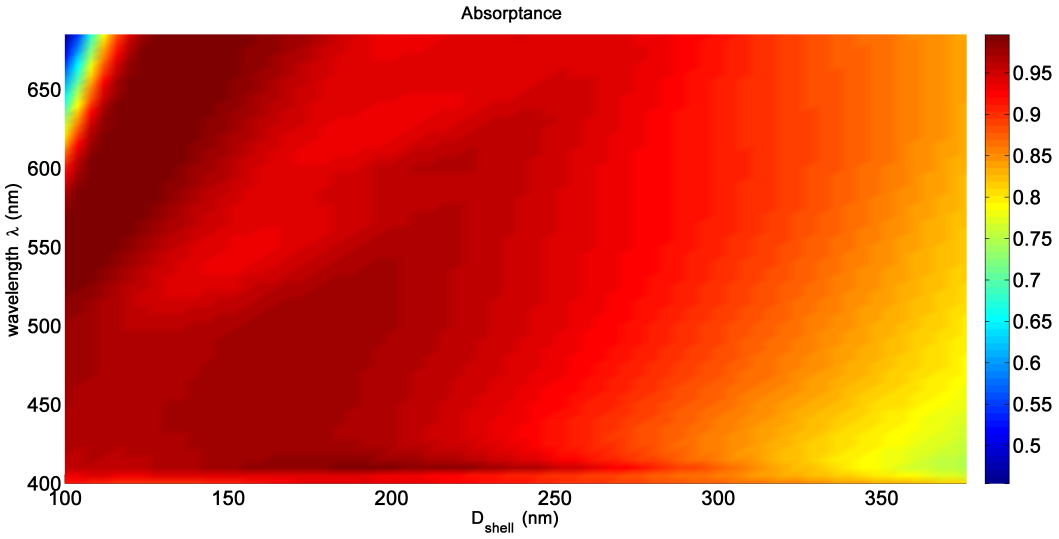

Figure 3.5: *Absorptance* spectrum for different shell diameters. The wavelength of the incoming light is varied between 400nm and 700nm. The period of the nanowire arrays is $L_x = L_y = 410$nm

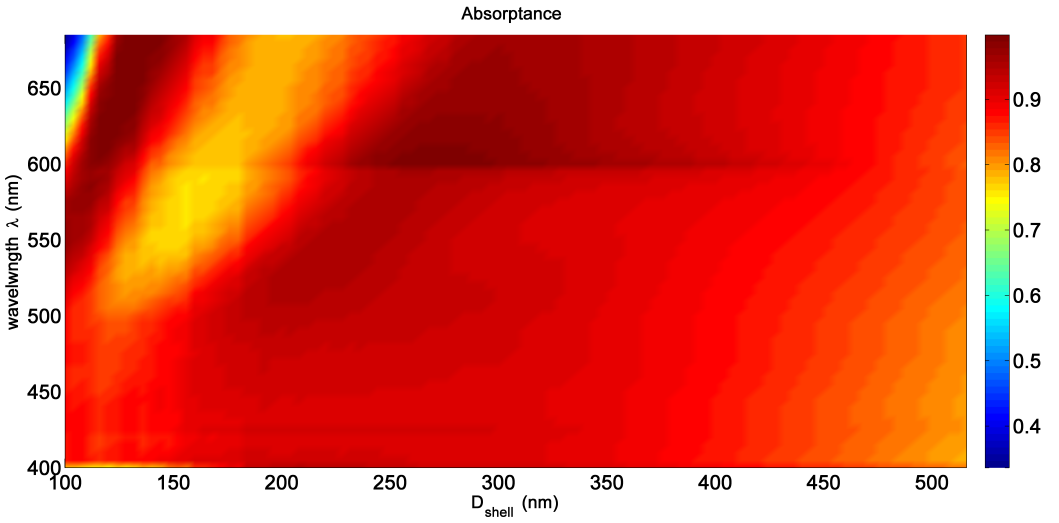

Figure 3.6: *Absorptance* spectrum for different shell diameters. The wavelength of the incoming light is varied between 400nm and 700nm. The period of the nanowire arrays is $L_x = L_y = 600$nm

previous argument. In this figure the shell diameter of the nanowires is

constant ($D_{shell} = 100$nm) and the *Absorptance* with the wavelength of the incoming light is plotted for different periodicities of the nano-structure. The peak in *Absorptance* appears at the same wavelength of the incoming light, for a certain shell diameter, when the period of the system is altered, which indicates that the peak originates from the absorption of the light by each individual nanowire.

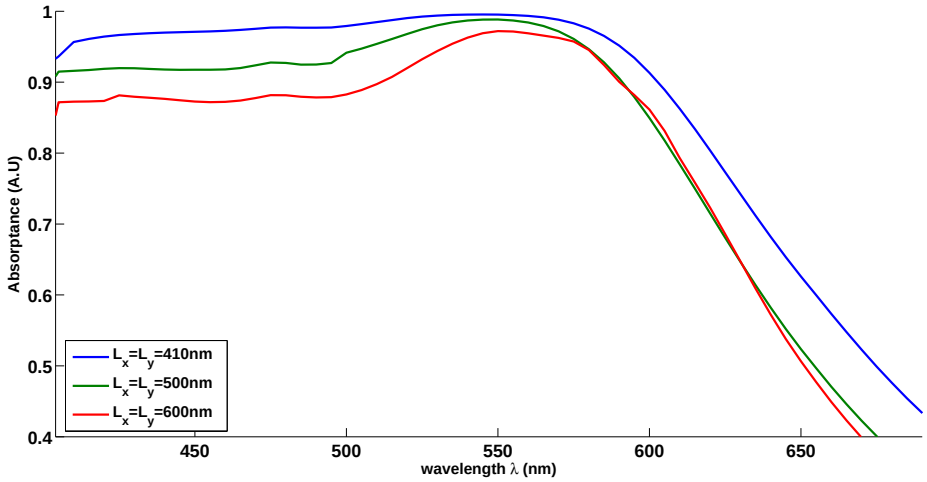

Figure 3.7: The plot of the *Absorptance* with wavelength of incoming light for different value of the period of the structure. The diameter of the nanowire is $D_{shell} = 100$nm.

The width of this area decreases as the period of the system increases and this is very clear in the figures 3.5, 3.1 and 3.6. This change of the width can be explained if we consider that in this particular area the excitation of the light propagation modes from the individual nanowires is the dominant absorption mechanism but it is not the only phenomenon that occurs. The coupling between nanowires, that exist in close vicinity, is also present in this area, co-existing with the phenomenon of the excitation of the propagation modes. As the period of the system increases the coupling becomes weaker and the area becomes narrower.

Furthermore, the next interesting observation from the three plots of the *Absorptance*, with different periods of the system, is that all three of them show a peak in *Absorptance* when the wavelength coincides with the value of the period of the nano-structure. This verifies that the structure acts as

a Bragg grating and traps the light. The most noticeable difference between the three diagrams, regarding this particular area, is that the position of the peak values in *Absorptance* corresponds to different values of the shell diameter of the nanowires, when the period is altered. The peak values of the *Absorptance* are observed at higher values of the shell diameter, as the period increases. More specifically, for the periodicity of 410nm the *Absorptance* exhibits maximum values when the shell diameter of the nanowires is between 180nm and 210nm($180nm \leq D_{shell} \leq 210nm$). For period $L_x = L_y = 500$nm the same area moves to higher values of shell diameter and is placed to diameter between 200nm and 230nm ($200nm \leq D_{shell} \leq 230nm$) and for period $L_x = L_y = 600$nm the area moves even more to shell diameter between 252nm and 292nm ($252nm \leq D_{shell} \leq 292nm$). The same observations can be made in the triangular area above this line of maximum *Absorptance*, where the *Absorptance* decreases as the wavelength of the incoming light increases. This triangular area also moves to higher values of the shell diameter of the nanowires, as the period increases. Thus, it is safe to conclude that the system presents maximum in *Absorptance*, which originates from the coupling between the nanowires, when the structure of the periodic arrays of nanowires is not too dense but also not too sparse.

3.2 Error Analysis

In this section the error that the computational calculations insert in the results is evaluated. The estimation, on how this error influences the results and the conclusions, is important for this error analysis. In every case of numerical computations, one has to take under consideration that a certain error is unavoidable, hence the reduction of this error to its minimum value it becomes a crucial point of the calculations. Especially, when the amount of data that needed to be handled is as large as the amount of data in the current work, this part of the reduction of the error is a very important and difficult venture.

On the other hand, apart from the reduction of the error, it is also important to estimate the error and describe how this error affects the results. This way it becomes possible to present the results properly and draw conclusions that interpret the results in a scientifically correct manner.

The computational calculations for this thesis are performed with a basis size $N_x = N_y = 21$ and all the results that are presented come from these

calculations. In order to estimate the error behaviour we repeat the calculations for different basis size and we compare the results. The largest basis size that we are in the position to use is $N_x = N_y = 27$ and this provides the most accurate result for this thesis.

The following figure shows the plot of the *Absorptance* spectrum, that corresponds to a nano-structure with periodicity $L_x = L_y = 500$nm and nanowire shell diameter $D_{shell} = 100$nm, for different basis sizes.

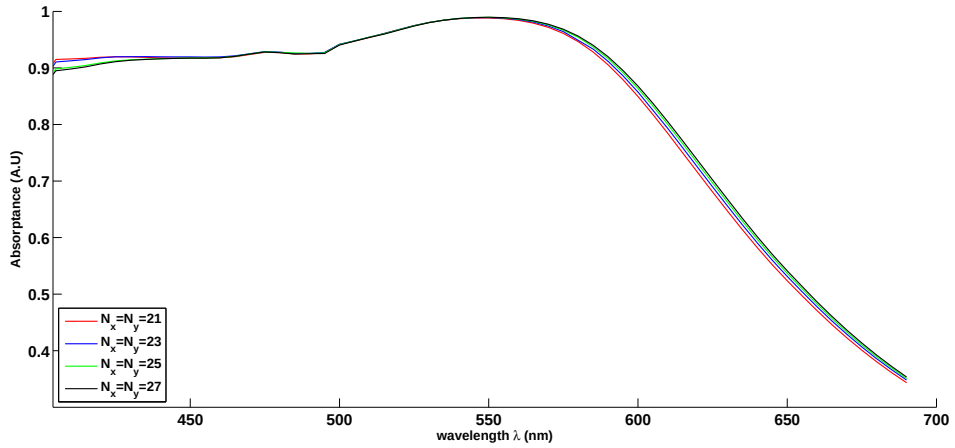

Figure 3.8: The plot of the *Absorptance* with wavelength of incoming light for different expansion basis sizes. The diameter of the nanowire is $D_{shell} = 100$nm and the period of the structure is 500nm.

The error is calculated by subtracting the value of the *Absorptance*, that we compute using basis size $N_x = N_y = 21$, with the value of *Absorptance* with the maximum accuracy that we are able to approach, by using basis size $N_x = N_y = 27$. This error presents a maximum value of approximately 0.02 A.U in the *Absorptance*. However, the error is not constant and in some areas of the *Absorptance* spectrum the results seem to converge, with very small deviations. In fig.3.8 it is verified that for some areas of the spectrum the results almost converge.

Furthermore, it is very important that the position of the peak does not change when a larger basis is used. This is important because the conclusions, that are presented in the previous section depend in a great extent on the position of the areas where the peak values of the *Absorptance* appear.

Since the results present a scientific consistency and a logical coherence, the accuracy of the position of the peak values of the *Absorptance* is a crucial point.

To sum up, the error inserts a level of uncertainty regarding the absolute values of the *Absorptance*; nevertheless, the fact that the shape of the diagrams seems to remain invariable to the change of the basis size allows us to draw very important conclusions about the mechanism of the light interaction with the nano-structure, that is studied.

3.3 Electric field distributions

The plots of the electric field distributions across different cross-sections of the system provide very important information regarding the propagation of light inside the system. Using these plots it becomes possible to determine which modes propagate inside the nanowires, how confined the electric field is inside the nanowires, how strong the electric field is or in which positions inside the nanowires the absorption of the light takes place.

Initially, the electric field distribution on the horizontal cross-section of the unit cell is plotted. The electric field is calculated in every position of the xy-plane of the unit cell and for certain positions along the z-direction. The objective is to study how the electric field distributions change as the light penetrates deeper inside the nanowire. It is assumed that the zero in z-axis coincides with the top of the nanowires, because the light is incident on top of the nanowire structure from the air, and as the light propagates inside the nanowire the variable z increases. For shell diameter $D_{shell} = 116$nm, period $L_x = L_y = 500$nm and wavelength of incoming light $\lambda = 605$nm the system presents very high *Absorptance* (*Absorptance* $= 0.9974$), hence, it is a very interesting case for studying the electric field distributions. In the following plots it can be seen how the electric field varies across the xy-plane of the unit cell, at different cross-sections of the system with the above mentioned characteristics.

The first set of plots (fig.3.9) shows the distributions of the y component of the electric field across the xy-plane, for different cross-sections of the nano-structure's unit cell along the z direction, at the positions: z=40nm, z=160nm, z=280nm, z=400nm, z=520nm and z=600nm.

The propagating modes described at the theoretical section of the thesis can be seen very clearly in these diagrams. The pattern of a superposition

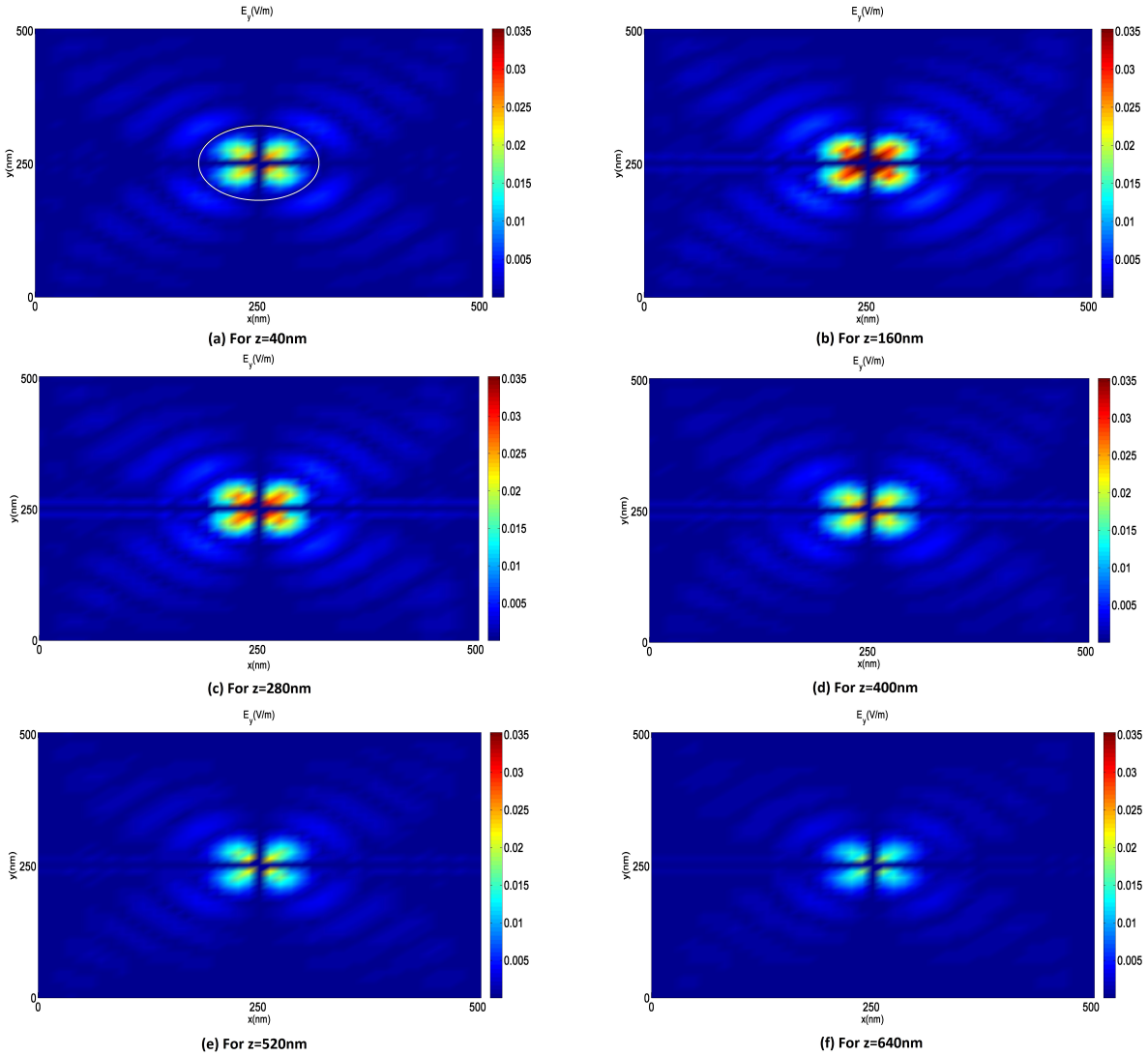

Figure 3.9: The y component of the electric field (E_y) distributions across the xy-plane, in different cross-sections of the unit cell, along the z direction. The structure that corresponds to these plots has a shell diameter of the nanowires D_{shell} = 116nm , periodicity $L_x = L_y$ = 500nm and the incoming light has wavelength $\lambda = 605$nm.

of resonant states is distinguishable. It is also obvious that the electric field is not confined inside the area of the nanowire, but it is distributed across

the whole area of the unit cell, forming these interference rings around the nanowire. The area of the nanowire cross-section is the area inside the circle in the fig.3.9(a).

Additionally, we can conclude that the electric fields of the light waves is gradually decreased as the light penetrates inside the structure. In figure 3.9(a), that corresponds to z=40nm, the maximum value of the electric field is $E_{y,max} = 0.0249$V/m, while deeper inside the nanowire, at the position z=160nm (fig.3.9(b)), we get a stronger electric field, $E_{y,max} = 0.0353$V/m. Propagating further inside the nanowire the light mode is losing energy, either because of the absorption or because it *leaks out* of the nanowire. For the positions z=280nm, z=400nm, z=520nm and z=640nm we calculate: $E_{y,max} = 0.029$V/m, $E_{y,max} = 0.0246$V/m , $E_{y,max} = 0.0216$V/m and $E_{y,max} = 0.0177$V/m, respectively. These values of the electric field for the different cross-sections indicate that it may be a standing wave formation along the z direction, since the electric field is weaker at the z=40nm cross-section compared to the electric field at the z=160nm cross-section.

In order to obtain a better understanding of the absorption along the z direction of propagation, it is very useful to plot the electric field distributions across the xz-plane (vertical cross-section of the unit cell of the nano-structure). In fig.3.10 the y component of the electric field distributions across the vertical cross-section of the nanowire, at the position y=210nm, is plotted. We continue studying the same system as before, with $D_{shell} = 116$nm, period $L_x = L_y = 500$nm and wavelength of incoming light of $\lambda = 605$nm.

This plot shows that the light is losing energy as it propagates inside the nanowire and the propagation of the light wave modes inside the nanowire is very clear. The electric field is gradually reduced as the light penetrates inside the nanowire, but the formation of the propagation mode seems to be preserved unchanged. However, after the first half of the nanowire a large percentage of the light energy seems to be absorbed and it is almost totally absorbed when the light reaches z=1600nm. These small values of the electric field are probably the reason why the formation of a standing wave along z is not clear from this plot.

To sum up, the previous plots allow us to conclude that across the plane perpendicular to the light propagation direction, the light forms resonant standing wave sates, that we call propagation modes. More specifically, these propagation modes are superpositions of these standing wave states and originate from the fact that the wavelength of the light is comparable

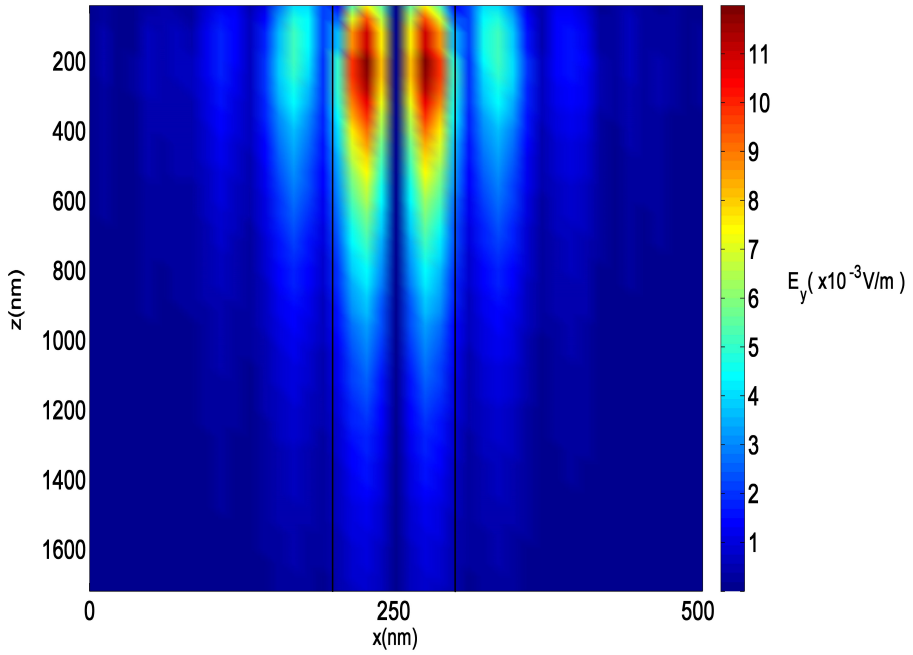

Figure 3.10: The distribution of the y component of the electric field across the xz-plane. This vertical cross-section is taken at the position y=210nm. The incoming light has wavelength $\lambda = 605$nm and the period of the system is 500nm. The area between the two black lines is the cross-section of the nanowire.

to the diameter of the nanowire. The nanowire acts as a propagation waveguide for the light. Additionally, the vertical cross-section of the unit cell provides information on how the light propagates along the z-axis.

Finally, the calculation of the x component of the electric field in the same nano-structure is performed. In fig.3.11 the electric field distribution across the xy-plane is plotted, for different horizontal cross-sections of the unit cell of the system. The plots do not seem to have a similar form with the y component of the electric field distribution plots. In these plots, we observe a very focused light beam in the middle of the nanowire. The x component has much higher value compared to the y component and it decays as the light penetrates inside the nanowire. The fact that the x component of the electric field has high values is perfectly reasonable, since the incoming light is assumed to be an x-polarized plane wave. The reduction of the electric field in the middle of the nanowire is also expected, due to the absorption of the light inside the nanowire.

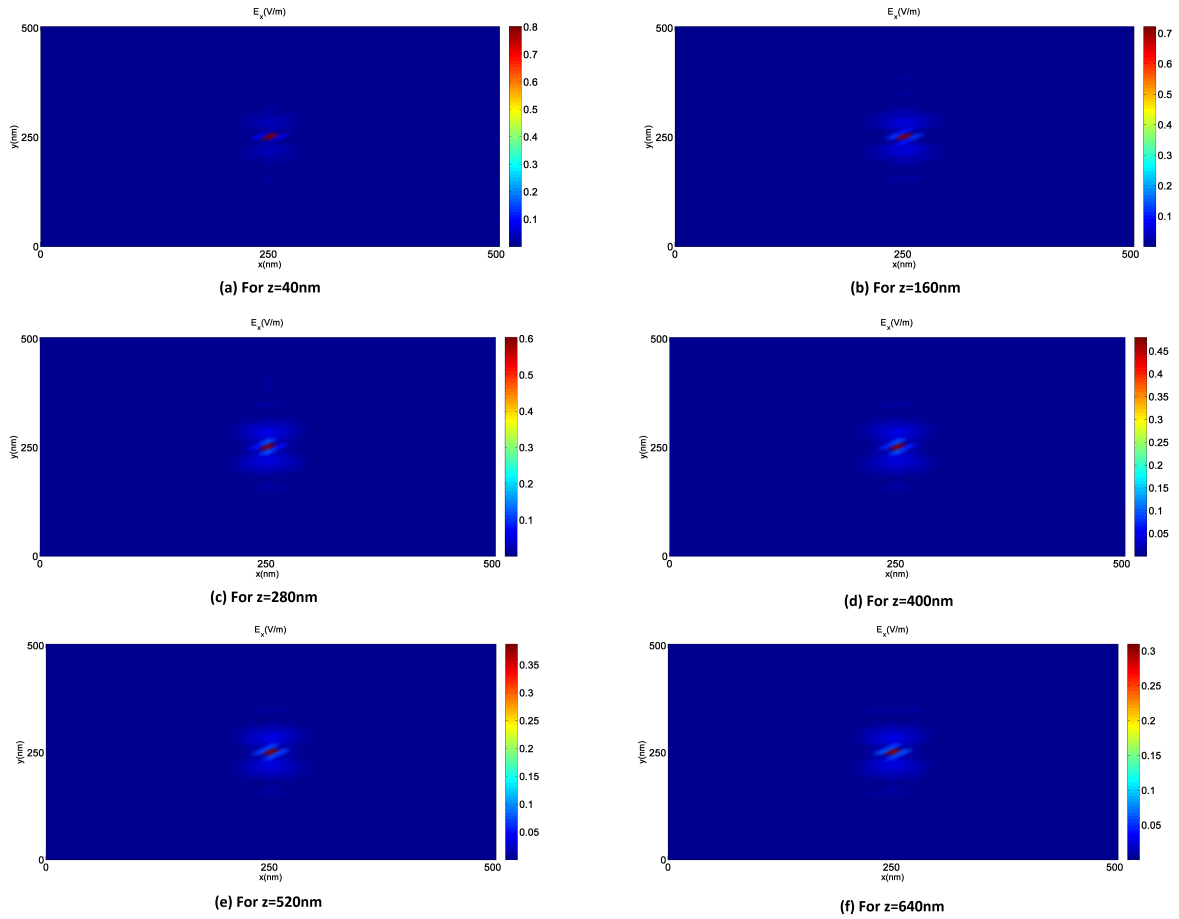

Figure 3.11: The x component of the electric field (E_x) distributions across the xy-plane, in different cross-sections of the unit cell, along the z direction. The structure that corresponds to these plots has a shell diameter of the nanowires $D_{shell} = 116$nm, periodicity $L_x = L_y = 500$nm and the incoming light has wavelength $\lambda = 605$nm.

The reason that the plots in fig.3.11 do not show the light propagation modes pattern, as expected, is that the electric field E_x in the middle has very high values compared to the values that it takes in the rest of the area of the unit cell. The propagation modes can become visible only if we set the maximum in the colormap scale of the diagram at a lower value. Hence, in fig.3.12 we can see the same plots with the fig.3.11, but in this case we

set the maximum value for the electric field at $E_x = 0.1\text{V/m}$ - instead of the value $E_x = 0.8\text{V/m}$, that is the maximum for the previous plots. This way we lose the information about the values of the electric field in the middle of the nanowires but the propagation modes of light become more pronounced and distinguishable. The same result may be achieved by using a logarithmic scale plot.

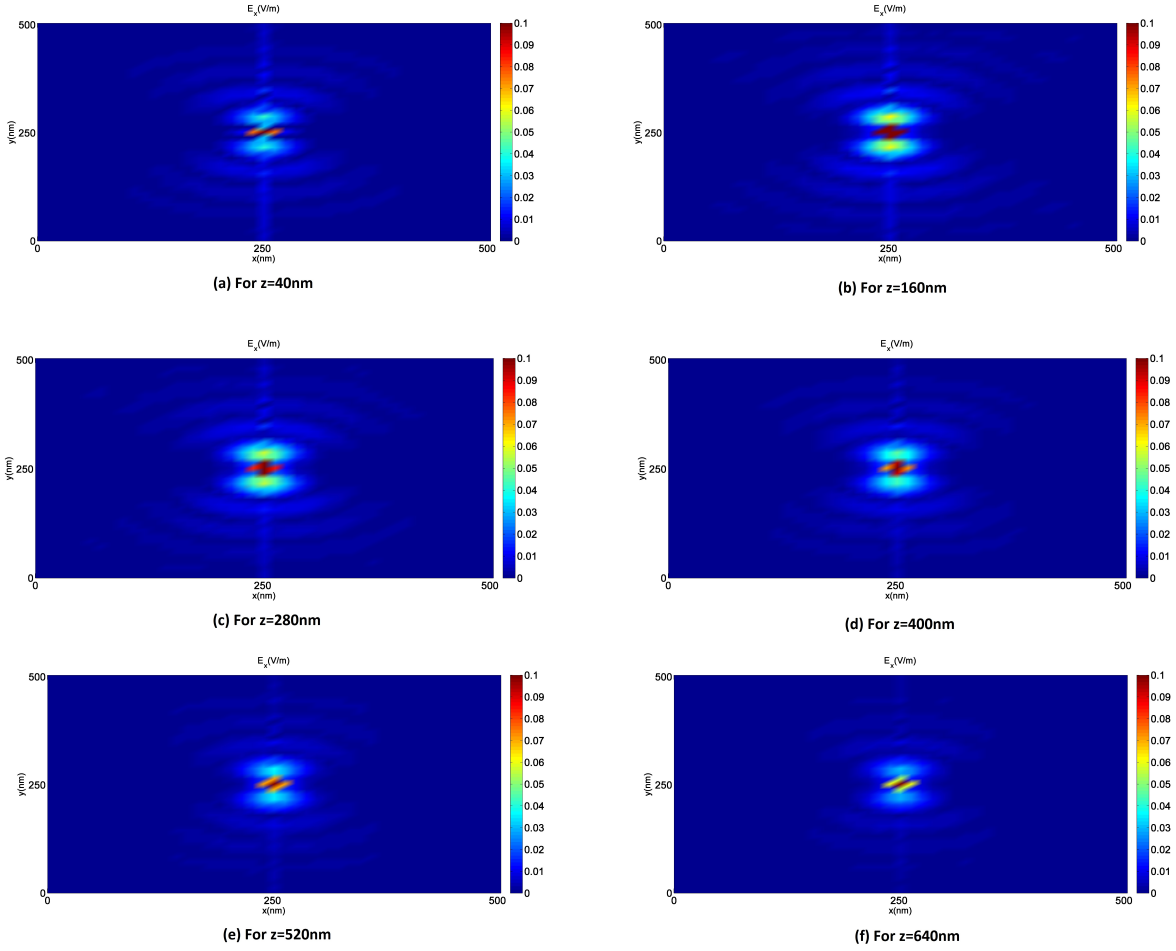

Figure 3.12: The x component of the electric field (E_x) distributions across the xy-plane, in different cross-sections of the unit cell, along the z direction. The maximum on the colormap scale is intentionally reduced in order to obtain a clearer picture of the light propagation modes.

Chapter 4

Conclusions-Outlook

This thesis work provides a description of the mechanisms that govern the light interaction with a nano-structure, constructed of periodic arrays of vertical core-shell nanowires. The information provided here allows us to extract important conclusions that help us to decide what geometrical design of the nano-structure is the most efficient for photovoltaic applications. Additionally, the results in the *Absorptance* values, that correspond to the wavelengths of the visible light spectrum, could be important for photo-detector applications.

Two main mechanisms of the light interaction with the nano-materials have an important impact on the *Absorptance* of the system. Firstly, the excitation of light propagation eigenmodes by the incoming light is the reason of the high values of the *Absorptance* that the system exhibits for certain wavelengths of this incoming light. This phenomenon originates by the absorbing behaviour of the individual nanowires and this is very clear from the plots presented in the results section of the thesis. Furthermore, the coupling of the electromagnetic field between neighbouring nanowires, or generally between nanowires that exist in close vicinity, constitutes the second mechanism responsible for the high values of the *Absorptance*.

The results regarding these two mechanisms are in agreement with previous publications on nano-structures consisting of periodical arrays of simple nanowires. However, the core-shell nanowire structure presents higher *Absorptance* values than the simple nanowire structures.

Lastly, another very important conclusion is that the *Absorptance* of the structure is decreased when the shell diameter of the nanowires is so large that the nanowires cover almost the entire surface of the nano-structure.

Consequently, a nano-structure consisted of nanowires with the shell diameter considerably shorter than the period of the structure is more efficient for a photovoltaic application. This conclusion allows us to reduce the material usage for the manufacture of the nano-structure and reduce the production cost of the photovoltaic devices.

A future step could be the creation of an improved algorithm, that enables us to use a larger expansion basis; this will result in an improvement of the precision of the computer calculations and the reduction of the computation time. The current results provide information that allows us to be confident about the above explained conclusions; however, it is necessary to verify the accuracy of these results by using a larger basis. More specifically, we should extend our error analysis with results from larger bases and if the results continue to show small deviations, similar to what we observe in the error analysis of the current thesis' results, we will be certain for the convergence of the results.

A logical continuation of the current thesis work could be to study different nano-structures. First of all, the combination of InAs, as the core material, and InP, as the shell material, is one of the many different combinations of semiconductor materials that we are able to choose for the construction of the core-shell nanowires. Placing the InAs in the core and GaAs at the shell or InSb at the core and GaSb at the shell could be some of the numerous material combinations for the structure of the core-shell nanowires.

Moreover, different geometries can be studied. The diameter of the nanowires could be varied along the arrays and the unit cell could be constructed of two or more nanowires with different diameters. It is also possible to replace the nanowires with nano-cones. All these changes could easily be done by simply changing a few lines of the algorithm.

It is also interesting if we can expand the *Absorptance* spectrum to a wider range of wavelengths of the incoming light. For this thesis the incoming light is assumed to be in the visible spectrum, with wavelengths between 400nm and 700nm. By implementing methods such as Fast Fourier Factorization or re-programming the algorithm in a different way, taking advantages of a higher level programming features, we could improve the speed of the calculations and make it possible to get more results.

Finally, the calculation of the ultimate efficiency η of the system in combination with *Absorptance* results could possibly be a very good suggestion for a better understanding of the phenomena.

Acknowledgements

I would like to thank my supervisor Prof. Hongqi Xu for giving me the chance to work in this very interesting subject. He was always very supportive and willing to answer every question and help with every problem. He taught me how to work in an extended project and I have acquired important experiences and knowledge during this one year that he supervised my thesis.

Moreover, I would like to thank Zhihu Yang, my supervisor's student to Peking University, for his important assistance. Nicklas Anttu, also, helped me understand some parts of his paper and I would like to thank him for that.

Finally, I would like to thank all my friends for their support. A special thank to Ali, Ali and Kasparas, whose help was valuable.

Self-reflection

During this year that I have been working for this thesis I acquired knowledge and experiences that I consider very important for my personal evolution and my professional career. With my supervisor's guidance I have learnt how to work in an extended project and how to deal with the problems that one needs to overcome in order to complete a research project. I became more confident on how to handle more advanced scientific questions and learnt how to overcome the difficulties of a project, by studying more deeply and get a profound understanding of the problem. The most important attainment from my work with the master thesis I consider to be the experience that I have gained on how to work on a theoretical scientific problem. Learning how to analyse a complex problem into smaller parts and after finding solutions for all the intermediate steps to synthesize them, in order to obtain a total solution, has been a valuable experience.

Furthermore, the knowledge that I acquired in the area of Photonics and in electrodynamics is very important. I have learnt how to apply mathematical methods in physical problems. The Fourier Modal Method and the Scattering Matrix Method, that I have used in order to solve Maxwell equations, represent two very important mathematical tools, that can be implemented in various physical problems.

Finally, I gained experience in computer programming and I have learnt the C programming language at a basic or maybe intermediate level. When I started this thesis, my computer programming experience was very poor and the fact that the thesis contained computer calculations was an additional motivation for me to choose this subject. I intended to improve my programming skills and it is in my plans to continue learning in this area, in order to be more confident in computer programming.

Bibliography

[1] N Anttu and H Q Xu. Scattering matrix method for optical excitation of surface plasmons in metal films with periodic arrays of subwavelength holes. *Physical Review B*, 83(16):165431, April 2011.

[2] Nicklas Anttu and H. Q. Xu. Efficient light management in vertical nanowire arrays for photovoltaics. *Optics Express*, 21:A558, 2013.

[3] D E Aspnes and A A Studna. Dielectric functions and optical parameters of Si, Ge, GaP, GaAs, GaSb, InP, InAs, and InSb from 1.5 to 6.0 eV. *Phys. Rev. B*, 27(2):985–1009, 1983.

[4] Jacques Bures. *Guided optics : optical fibers and all-fiber components*, volume 2. Weinheim : Wiley-VCH, 2009.

[5] H.R.Philipp. *Handbook of Optical Constants of Solids*. Edited by E.D.Palik, Academic,Orlando,FL, 1985.

[6] H. Kim, J. Park, and B. Lee. *Fourier Modal Method and Its Applications in Computational Nanophotonics*. Taylor & Francis, 2012.

[7] K. Knop. Rigorous diffraction theory for transmission phase gratings with deep rectangular grooves, 1978.

[8] David Ko and J. Inkson. Matrix method for tunneling in heterostructures: Resonant tunneling in multilayer systems. *Physical Review B*, 38(14):9945–9951, November 1988.

[9] Lifeng Li. A Modal Analysis of Lamellar Diffraction Gratings in Conical Mountings. *Journal of Modern Optics*, 40(4):553–573, April 1993.

[10] Lifeng Li. New formulation of the Fourier modal method for crossed surface-relief gratings, 1997.

[11] Zhi-Yuan Li and Lan-Lan Lin. Photonic band structures solved by a plane-wave-based transfer-matrix method. *Physical Review E*, 67(4):46607, April 2003.

[12] Eero Noponen and Jari Turunen. Eigenmode method for electromagnetic synthesis of diffractive elements with three-dimensional profiles, 1994.

[13] Bahaa E. A. Saleh and Malvin Carl Teich. *Fundamentals of Photonics*. Wiley, 2nd edition, 2007.

[14] T. P. White, L. C. Botten, C. Martijn de Sterke, R. C. McPhedran, A. A. Asatryan, and T. N. Langtry. Bloch mode scattering matrix methods for modeling extended photonic crystal structures. ii. applications. *Phys. Rev. E*, 70:056607, Nov 2004.

[15] Hongqi Xu. Scattering-matrix method for ballistic electron transport: Theory and an application to quantum antidot arrays. *Physical Review B*, 50(12):8469–8478, 1994.

[16] Hongqi Xu. Electron transport through one-dimensional lateral surface superlattices in magnetic fields. *Physical Review B*, 52(8), 1995.

[17] Lebo Zhang, P Brusheim, and H Q Xu. Multimode electron transport through quantum waveguides with spin-orbit interaction modulation: Applications of the scattering matrix formalism. *Phys. Rev. B*, 72(4):45347, July 2005.

[18] Lebo Zhang, Feng Zhai, and H Xu. Scattering matrix method for multimode electron transport through quantum wires under a local magnetic field modulation and spin-orbit interaction. *Physical Review B*, 74(19):195332, 2006.